Case Study: Effects of Wildfires on the Vertical Atmospheric Temperature Structure – New Insights with Satellite Data?

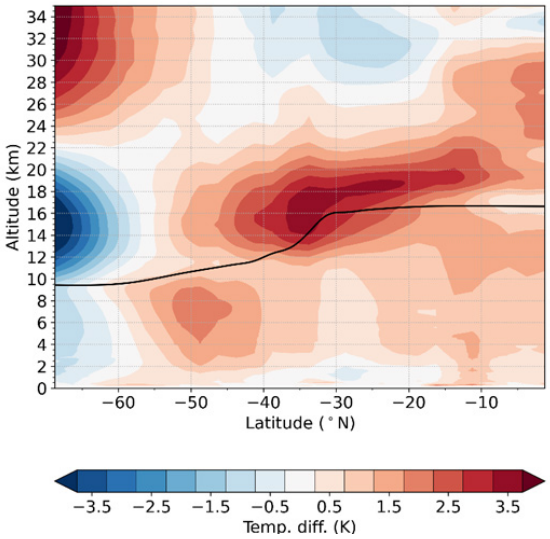

January 2021

Matthias Stocker & Andrea K. Steiner (Supervisor)

Wegener Center for Climate and Global Change, University of Graz

Funded by:

Commission Climate and Air Quality of the Austrian Academy of Sciences

Report content

Study report summarizing the results of the KKL-ÖAW-funded study “Fallstudie: Auswirkungen von Waldbränden auf die vertikale atmosphärische Temperaturstruktur – Neue Einblicke mit Satellitendaten?” (Nov.-Dez.2020)

Authored by

Matthias Stocker, MSc. (Study Scientist, Reiherstadlgasse 27, 8020 Graz, Austria)
Prof. Andrea K. Steiner (Study Supervisor, Wegener Center, University of Graz)
Wegener Center for Climate and Global Change, University of Graz, Brandhofgasse 5, 8010 Graz, Austria, http://www.wegcenter.at

Corresponding Author Contact: matthias.stocker@sbg.at

Commissioned & Funded by

KKL-ÖAW – Kommission Klima und Luftqualität der Österreichischen Akademie der Wissenschaften (Commission Climate and Air Quality of the Austrian Academy of Sciences)
Website: www.oeaw.ac.at/kkl

Graz, January 2021

Abstract

This case study examines the impact of wildfires on the thermal structure of the atmosphere. Two exemplary events are investigated, the Northern American wildfires in 2017 and the Australian wildfires in 2019/20. Aerosol measurements are used to track the movement and the extent of the aerosol clouds. Vertically high-resolved radio occultation (RO) observations reveal the effects on stratospheric temperature and short-term climate.

The results show substantial warming anomalies of about 4 K up to 10 K in the lower stratosphere, as observed in daily RO temperature profiles located within the wildfire plumes. The aerosol clouds are found to rise several kilometers in the stratosphere in just a few days. Cloud top heights are detected between 16 km and 24 km from RO consistent with those from aerosol data.

Furthermore, short-term climate signals of the wildfires were found larger compared to climate signals from the Calbuco volcanic eruption in 2015, one of the largest eruptions in the 2000s. Short-term climate signal estimates are about 1 K for the Northern American wild fires and up to 3.5 K for the Australian wildfires.

The study demonstrates that novel satellite observations from RO can provide new insights on the influence of wildfires on short-term climate change. The findings will be helpful for reducing uncertainties, particularly in stratospheric temperature trend detection.

Table of Contents

1. Introduction and objective

Forest fires influence the climate system by changing the surface albedo and releasing trace gases such as carbon dioxide but also aerosols. The latter have a direct or indirect influence on the radiative fluxes in the atmosphere by changing cloud properties and atmospheric chemistry (Langmann et al., 2009). One aspect that has received little attention so far is the impact of large wildfires on the stratosphere. There, the emitted aerosols are distributed globally and linger for months to years, potentially affecting climate in the short term (Fromm et al., 2010).

Intense fires can also trigger deep convection, which in extreme cases leads to the formation of pyrocumulonimbus clouds (pCb) and carries the combustion products up into the stratosphere (Paugam et al., 2016). In addition, intense wildfires, such as those in North America in 2017 or Australia in 2019/20, were observed to alter regional Stratospheric Aerosol Optical Thickness (SAOD) and regional radiative forcing as well as stratospheric ozone concentrations in ways that were previously only known from moderate to large volcanic eruptions (Ansmann et al., 2018; Yu et al., 2019; Khaykin et al., 2020).

Modelling studies show that in a warming climate intense fires will occur more frequently (Flannigan et al., 2013). This suggests that wildfires will become an increasingly relevant aspect of near-term climate change. Currently, however, there are still large uncertainties regarding the impact of intense fires on climate.

In this case study, the impact of wildfires on the thermal structure of the atmosphere is investigated for two exemplary wildfires. The focus is on their effect on the upper troposphere and lower stratosphere using satellite-based Radio Occultation (RO) observations to track the evolution of wildfire aerosol plumes from day-to-day and to estimate the short-term climate impact.

Two major wildfire events, the Australian wildfires 2019/20 and the Northern American wildfires in 2017 are investigated using vertically high-resolved RO data in combination with different aerosol measurements. New insights into changes of the regional vertical atmospheric temperature structure following these two large fires are presented.

An additional focus is given on the applicability of RO data for detecting the influence on the vertical temperature structure as well as the maximum impact altitude of the wildfire events. Furthermore, the current resolution limits of RO for observing wildfires and their future potential for observing smaller events is discussed.

2. Data and methods

This Section gives an overview of data and methods used to determine the imprints of large wildfires in the stratospheric temperature.

2.1. Radio occultation data

The Global Navigation Satellite System (GNSS) Radio Occultation (RO) is an active limb sounding technique where radio-waves from GNSS satellites are utilized for remote sensing of the atmosphere (Steiner et al., 2011; Anthes 2011). During an occultation event the atmosphere is vertically scanned and bending angle profiles are calculated from phase measurements. These form the basis for the derivation of vertical profiles of key atmospheric parameters such as refractivity, pressure, geopotential height, temperature, and humidity. Their long-term stability and low structural uncertainties make them especially favorable for climate studies and trend detection (Steiner et al., 2013; Stocker et al., 2019; Steiner et al., 2020).

In this study, the multi-satellite record from the Wegener Center (WEGC) Occultation Processing System version 5.6 (OPSv5.6) (Schwärz et al., 2016; Angerer et al., 2017; EOPAC Team, 2019) is used. Individual temperature profiles as well as gridded monthly-mean temperature data on a 2.5°x2.5° latitude/longitude grid are utilized.

From the individual profiles as well as the gridded monthly-mean temperature anomalies are calculated for individual profiles as well as gridded monthly-mean profiles by subtracting the seasonal cycle, i.e., monthly means for the reference period 2002 to 2019. Anomalies of the RO profiles are generated by subtracting the values of the nearest grid point in the 2.5°x2.5° latitude/longitude reference climatology for the corresponding month from the individual profile. Only high-quality RO profiles (QF 0) are considered.

2.2.Aerosol data

To keep track of the wildfire aerosol clouds, different aerosol measurements from different instruments are used in this study. The UV-Aerosol Index (AI) data as provided by the Ozone Measuring Instrument (OMI) on board of the Aura satellite is used to locate the wildfire plumes in the horizontal while the Volume Extinction Coefficient (VEC) data as provided by the Ozone Mapping and Profiler Suite Limb Profiler (OMPS-LP) are used to track the wildfire plumes in the vertical. For the intercomparison of the short-term climate signals with the perturbation in the stratospheric aerosol concentration, the VEC

measurements from the high-resolved Global Space-based Stratospheric Aerosol Climatology (GloSSAC) are utilized.

OMI/Aura UV-Aerosol Index (AI) data

The OMI/Aura UV-AI can be used to detect the presence of UV absorbing aerosols such as soot. It also allows to discriminate between different types of aerosols. Positive AI values indicate the presence of e.g., volcanic aerosols or smoke aerosols while close to zero and negative values indicate clouds or weakly absorbing aerosols such as sea salt (Ansmann et al., 2018; Hammer et al., 2016). This information, in combination with satellite images in the visible range (e.g., MODIS), allows a discrimination between water clouds and the aerosol plume.

In this study, OMI/Aura UV-AI data with a daily resolution on a 1°x1° longitude/latitude grid are used (Torres, 2006). The data are available from the Goddard Earth Sciences Data and Information Services Center (GES DISC)[1].

OMPS-LP aerosol data

OMPS-LP is a limb profiler onboard the Suomi-NPP satellite which detects limb scattered sunlight and flies in a sun-synchronous orbit. It orbits the earth about 14.5 times a day and takes vertical profiles of the atmospheric limb every 125 km along track (Zawada et al., 2018).

The processed OMPS-LP Level 2 aerosol product used in this study provides the stratospheric aerosol VEC for an altitude of about 6.5 km to about 30 km at a 1 km vertical grid on a daily basis. The data offer a near global coverage from 82°S to 82°N.

OMPS-LP L2 aerosol data used in this study are processed and made available by the University of Saskatchewan[2].

GloSSAC aerosol data

The GloSSAC is a continuous gap free aerosol climatology constructed from measurements of ground- or balloon-based instruments as well as different spaceborne instruments such as the Stratospheric Aerosol and Gas Experiment (SAGE), Optical Spectrograph and InfraRed Imaging System (OSIRIS), Cloud-Aerosol Lidar and Infrared Pathfinder Satellite Observation (CALIPSO) (Thomason et al., 2018).

[1] OMI/Aura data: https://disc.gsfc.nasa.gov/datasets/OMAERUVd_003/summary
[2] OMPS-LP data: https://arg.usask.ca/projects/omps-lp/

GloSSAC v2.0 also incorporates also latest data from SAGE III on the International Space Station and covers the time-range from 1979 to 2018 (Kovilakam et al., 2020).

The main variable used in this study is the monthly mean VEC at a wavelength of 525 nm on 5°-zonal bands which cover the latitude range between 80°N and 80°S. In the vertical it covers the atmospheric layer from the tropopause to 40 km altitude with a resolution of 500 m (Thomason et al., 2018; Kovilakam et al., 2020). In addition to the VEC, a measure for the stratospheric background is also included in the data set. It represents the average monthly VEC averaged over the years 1999 to 2004, excluding 2002 (Thomason et al., 2018). The GloSSAC v2.0 is publicly available from the NASA Atmospheric Science Data Center[3].

2.3. Determining the evolution of the wildfire plumes

The wildfire plumes are tracked using MODIS corrected reflectance satellite images in the visible range as well as the OMI/Aura UV-AI. In the vertical, the cloud top altitude is determined from the RO temperature anomaly profiles. Only those profiles are considered, which are located within the centre of the aerosol cloud (defined as the region where the UV-AI exceeds a value of 3) and exhibit a warming peak larger than 3 K in the lower stratosphere. Starting from the altitude of the maximum lower stratospheric warming peak the local temperature minimum above is detected. The altitude of this minimum is then defined as cloud top altitude.

The volcanic cloud top altitude derived from the RO data is compared to the cloud top altitude derived from OMPS-LP aerosol measurements for the corresponding region. For the OMPS-LP data, the cloud top altitude is defined as the altitude where the VEC drops below a value of 0.001.

This is a relatively simple approach, however, as will be shown in the results section (Sect. 3.1.2, Fig. 11), the altitudes derived from the RO anomaly profiles as well as the OMPS-LP aerosol data show a high correlation, which confirms the utility of RO for cloud top detection and shows top heights of aerosol clouds in the lower stratosphere. This is supported by Khaykin et al. (2020; Fig. 5 therein) indicating that the top height of the aerosol cloud for the 2019/20 Australian wildfires is connected to the cooling above the maximum warming peak in the lower stratosphere.

A more sophisticated approach to derive cloud tops from RO measurements is used by Biondi et al. (2013) and Biondi et al. (2017), which is based on bending angle profiles collocated with CALIPSO aerosol data to determine the maximum cloud top height of tropical cyclones and of volcanic plumes,

[3] GloSSAC data: https://asdc.larc.nasa.gov/data/GloSSAC/GloSSAC_V2.0.nc

respectively. Such an approach may be favoured in a longer-term study on the atmospheric impacts of forest fires in the future.

2.4. Determining short-term climate imprints of wildfires

For the detection of the short-term climate imprints in the atmospheric thermal structure 2.5°-latitude bands are created from the monthly mean gridded (2.5°x2.5° latitude/longitude) RO temperature anomalies. Then, the mean is taken over three months before the event and three months after the event. Finally, the difference is calculated between the mean temperature before and after the event, which corresponds to the temperature signal of the event. Note, that the definition of the three-months pre-event mean versus the three-months post-event mean was chosen to provide some degree of comparability between the two investigated wildfire cases and due to the availability of RO data until March 2020 only.

Please note that variability modes other than the seasonal cycle, such as the Quasi-Biennial Oscillation (QBO) or El Niño–Southern Oscillation (ENSO), which could be the subject of a more thorough study of this topic, have not been considered. However, QBO is mainly relevant in the tropical and subtropical region. In addition, there were no major ENSO events during the periods studied.

3. Results

3.1. The evolution of wildfire plumes and the impact on the vertical temperature structure

This section presents the results of the daily tracking of the North American wildfire development in 2017 that affected the Northern Hemisphere and of the record-breaking Australian wildfire events in 2019/20 that affected the Southern Hemisphere. Focus is on gaining knowledge about the impact of wildfires on stratospheric temperature and on assessing the potential of Radio Occultation (RO) in this context.

3.1.1. Evolution of the 2017 Northern American wildfire plume

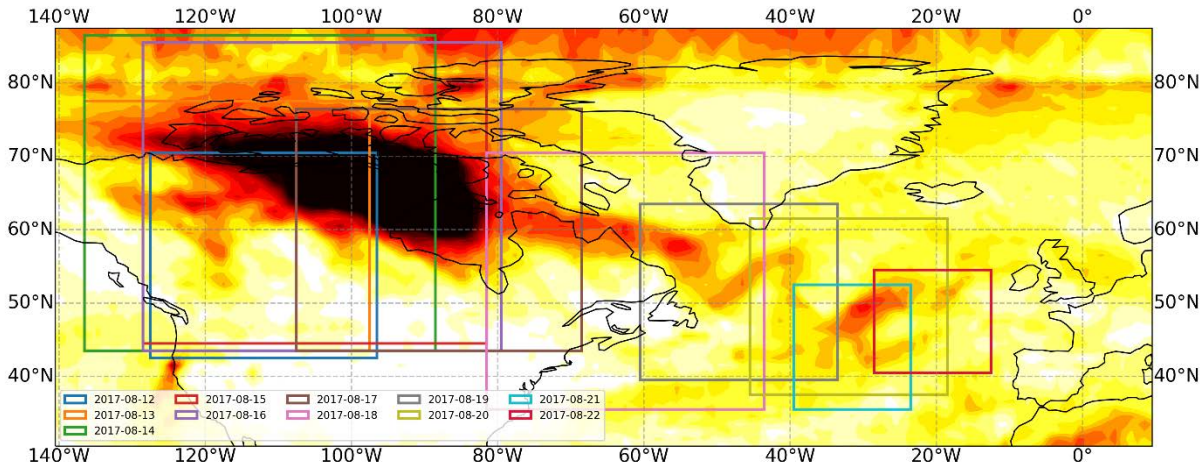

Figure 1: Mean Aerosol Index (AI) for the 2017 Northern American wildfire event between Aug. 12 and Aug. 22. The colored rectangles show the area that was examined on the respective days. AI values range from 0 to >10 (white to black).

The Northern American wildfires started on Aug. 12, 2017 and several pCb plumes formed a vast aerosol cloud. According to Peterson et al. (2018) the aerosol cloud reached the stratosphere on Aug. 14. In the following the cloud was transported eastwards by the polar jet stream and cycled the globe within a few weeks.

As shown in Fig. 2, a massive aerosol plume developed on Aug. 12 between 55°N to 65°N and 115°W to 125°W. The RO profiles co-located with the plume indicate a strong tropospheric warming which is accompanied by a strong cooling in the tropopause region (horizontal dashed lines). However, it is yet

not clear whether this structure is caused by the wildfire aerosols or the tropospheric weather conditions. On the following days, the area covered by the plume increased, most likely to additional pCb events (Peterson et al., 2018).

Some of the RO profiles co-located with the plume (e.g., Fig. 2, Aug. 12, and Aug. 13), also show a relative warming peak (compared to the strong cooling) above the tropopause which may be explained by wildfire aerosols reaching the lowermost stratosphere, although the OMPS aerosol data (Fig 2, far right) do not show a strong stratospheric perturbation. Yet, as visible in Fig. 2 the OMPS-LP measurements did not directly probe the central part of the aerosol clouds on Aug. 12 and 13.

CALIPSO data, as shown by Peterson et al. (2018), indicate that on Aug. 14 the aerosol plume already reached the stratosphere at latitudes around 70 °N. However, a relative warming signature cannot be observed in the RO profiles for Aug. 14 (Fig. 2, bottom). But in this case the RO profiles mainly probed the borders of the aerosol plume and there are no profiles available for the central area.

Between Aug. 14 and 15, most of the wildfire plume started to drift eastwards, reaching the Northern Atlantic coast on Aug. 18. On Aug. 19, as the plume reaches the Atlantic Ocean, a distinct relative warming, peaking at an altitude around 15 km, manifests in the lower stratosphere (see. Fig. 3). This pattern indicates a strong warming effect of stratospheric aerosols at the respective altitudes.

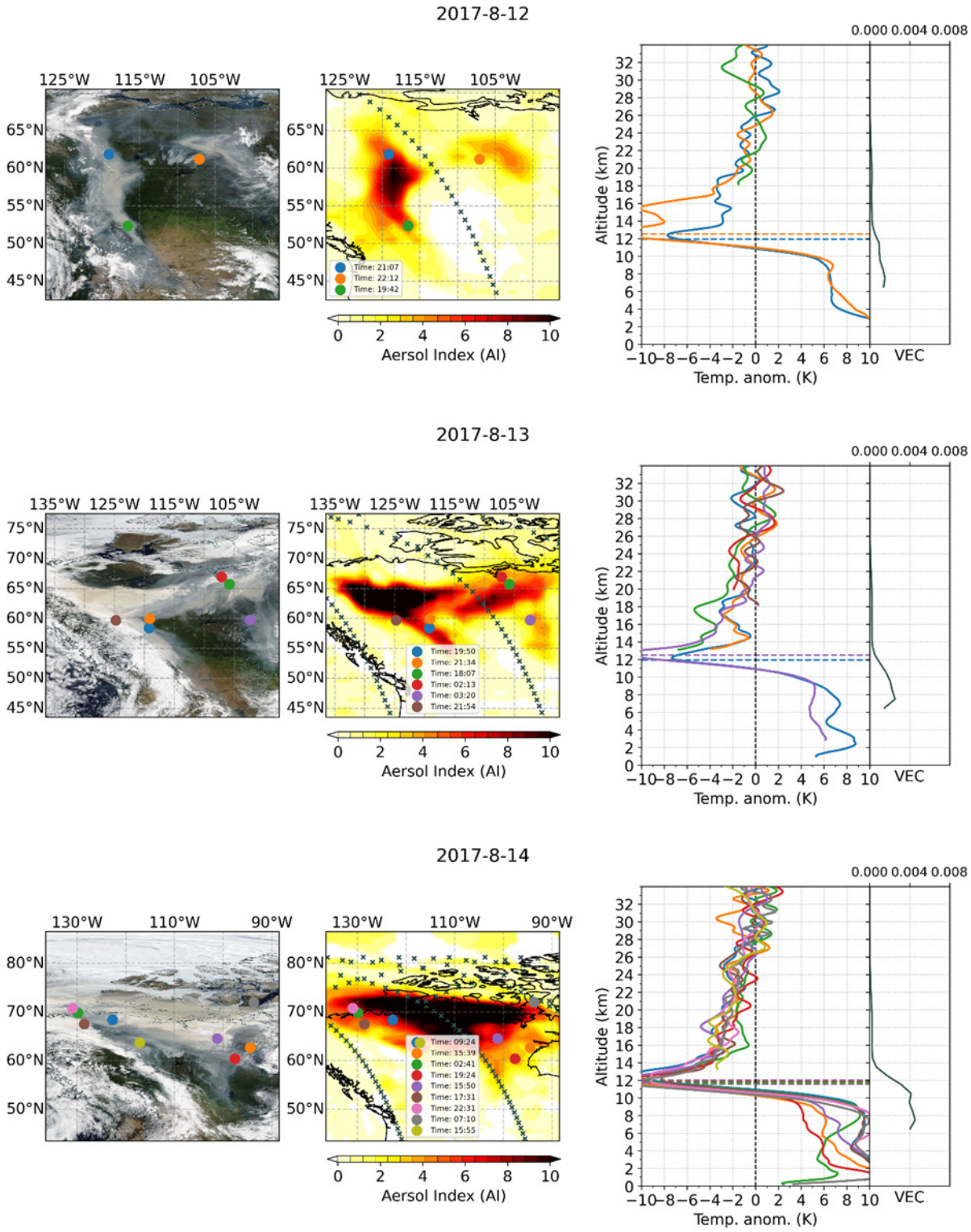

Figure 2: MODIS satellite image (left), Aerosol Index (AI) (center) and RO temperature anomaly profiles (right) as well as OMPS-LP aerosol data (VEC; right subpanel) for the examined area on Aug. 12, 13 and 14 (top to bottom). Colored dots represent the locations of the RO-measurements. Black crosses in the central plots indicate the locations of the OMPS-LP measurements. Horizontal colored dashed lines in the right plots indicate the lapse rate tropopause for the individual profiles.

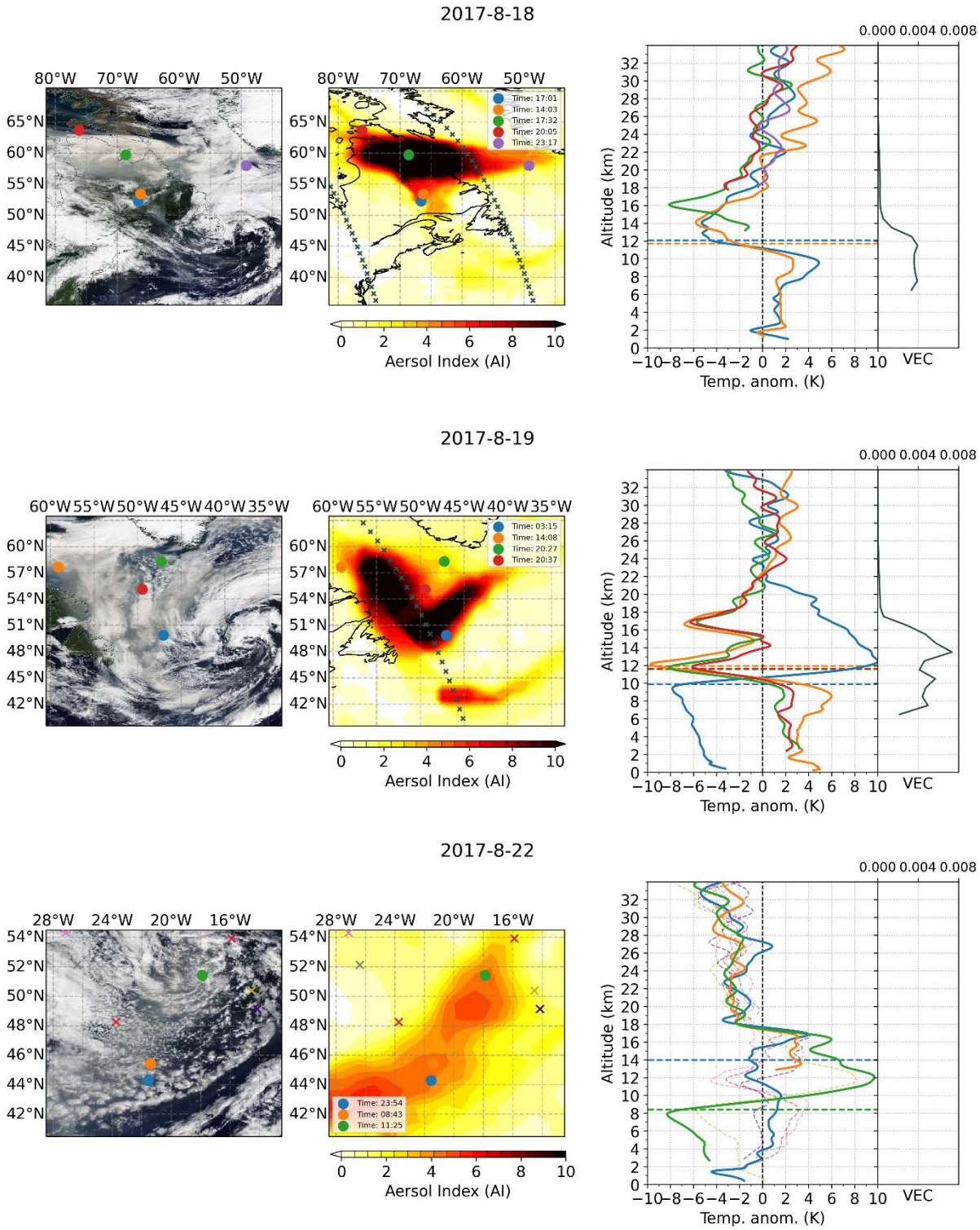

Figure 3: MODIS satelite image (left), Aerosol Index (AI) (center) and RO temperature profiles(right) as well as OMPS-LP aerosol data (VEC; right subpanel) for the examined area on Aug. 18, 19 and 22. Colored dots and x icons represent the locations for the RO-profiles inside and outside the aerosol plume, respectively. Black crosses in the central plot indicate the locations of the OMPS-LP measurements. Horizontal colored dashed lines in the right plots indicate the lapse rate tropopause for the individual profiles.

The following days, the wildfire plume was transported across the Atlantic Ocean by a low-pressure system and reached the European continent on Aug. 22 (see Fig. 3). Ansmann et al. (2018) found a strong distortion of the lower stratospheric aerosol concentration over central Europe, with a cloud top altitude of ~16 km. This is consistent with the top height found in this study (Fig. 3 bottom).

Most of the RO profiles co-located with the plume during its journey across the Atlantic exhibit a strong warming in the lower stratosphere of up to almost 10 K. Depending on the latitude the stratospheric warming extends up to 18 km in agreement with the aerosol concentration reported by OMPS-LP measurements (Fig.3, right subpanel). Profiles outside the central area of the aerosol cloud also show a warming of the lower stratosphere, albeit to a lesser extent. This indicates that the aerosols have already been distributed over a larger area. This is in line with Fig. 1 which shows increased AI values for a broad latitude range during the investigated period.

Another plausible explanation for the lower stratospheric warming signals could be deep convection (Johnston et al., 2018). This, however, seems unlikely in the investigated case, since the warming extends deep into the stratosphere and persists in areas with a weak cloud cover (e.g., Aug. 22, Fig. 3 bottom). Additionally, in northern hemispheric mid to high latitudes, storms causing deep convection with the potential to affect the stratosphere are mainly observed over land surface (Liu & Liu, 2016) while here the main warming signals are observed over ocean areas.

Figure 4 displays the daily-mean of the RO temperature anomaly profiles co-located with the aerosol cloud for the ten days during the event. The results show that a strong lower stratospheric warming develops on Aug. 19 as the plume reaches the Atlantic Ocean and persists until Aug. 22. During those days, the plume rises from ~16 km to ~18 km.

Following Aug. 22, the AI drops below the threshold of 3. Since this study primarily focuses on a proof of concept, the evolution was not tracked further. However, as described by Peterson et al. (2018) the aerosol plume persisted in the stratosphere and cycled the globe within a few weeks. Therefore, it is very likely that the cloud also influenced the stratospheric temperature after Aug. 22.

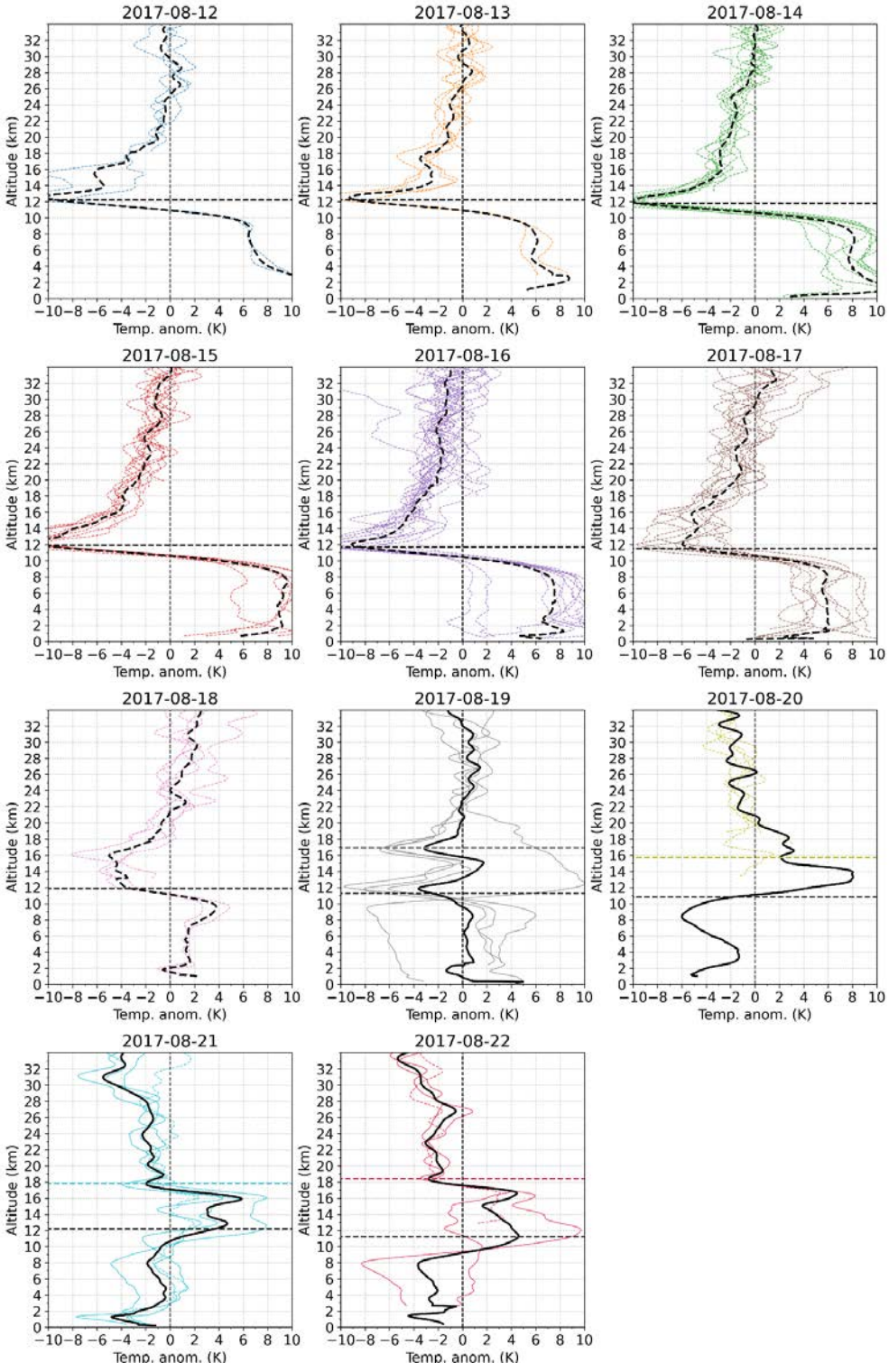

Figure 4: RO temperature profiles within the wildfire aerosol cloud (colored) and the mean temperature profile (black) for each day for 12–22 Aug. 2017. The color-code refers to the different regions examined on the individual days (see Fig. 1). The horizontal black dashed line denotes the mean lapse rate tropopause while the colored dashed horizontal line denotes the estimated plume top altitude. Profiles which do not show a peak exceeding 3 K are dashed and were not considered for the calculation of the mean value.

3.1.2. Evolution of the 2020 Australian wildfire plume

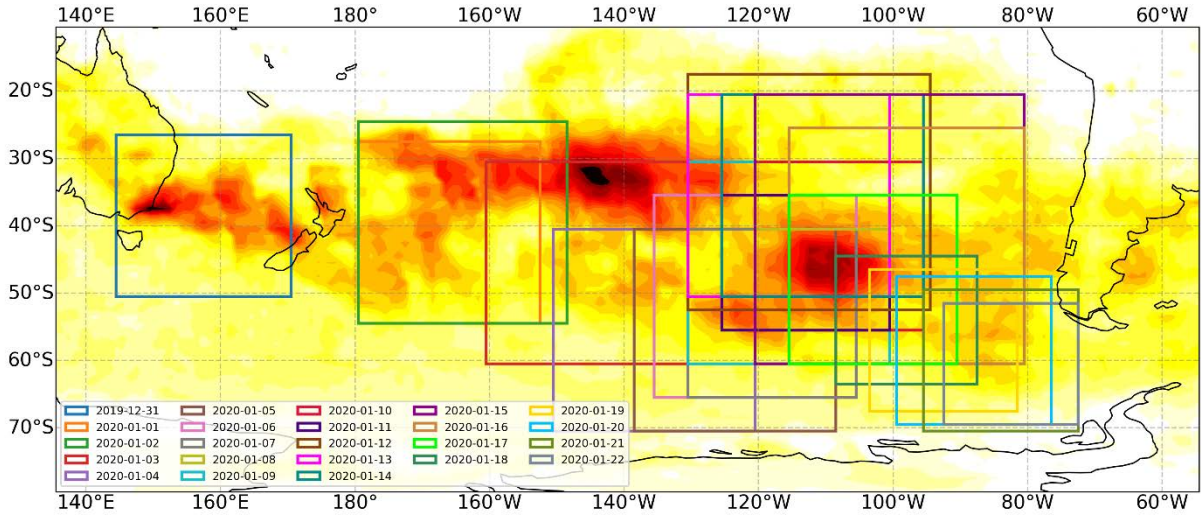

Figure 5: Mean Aerosol Index (AI) between Dec. 31 and Jan. 22 for the 2019/20 Australian wildfire events. The colored rectangles show the area that was examined on the respective days. AI values range from 0 to >10 (white to black).

The evolution of the 2019/20 Australian wildfires is displayed in Fig. 5. During their progression two major pCb outbreaks took place (Khaykin, et al., 2020). The first major event started on Dec. 31, 2019, where a massive aerosol cloud evolved slightly southeast of the Australian coast in both, the UV-AI map as well as the MODIS satellite image (Fig. 6). OMPS-LP measurements also exhibit a highly elevated aerosol extinction in the upper troposphere for the corresponding region. The RO profiles co-located with the aerosol cloud indicate a strong warming affecting the whole troposphere. Also, a negative temperature anomaly can be identified as has been also observed for the 2017 Northern American wildfires. As already discussed in Sect. 3.1.1, a warming of the aerosol cloud as well as the prevailing weather conditions appear to be a reasonable cause for this structure. On Jan. 1, the cloud has already been transported eastwards, and some of the RO profiles co-located with the aerosol cloud show a relatively strong warming in the lower stratosphere at an altitude of 20 km (e.g., Fig. 6, Jan. 1, red profile). Similar to the observations on the first days of the Northern American wildfires, OMPS-LP data show only a slightly elevated aerosol extinction at this altitude which makes it difficult to clarify whether this warming in the lower stratosphere is caused by the wildfire plume.

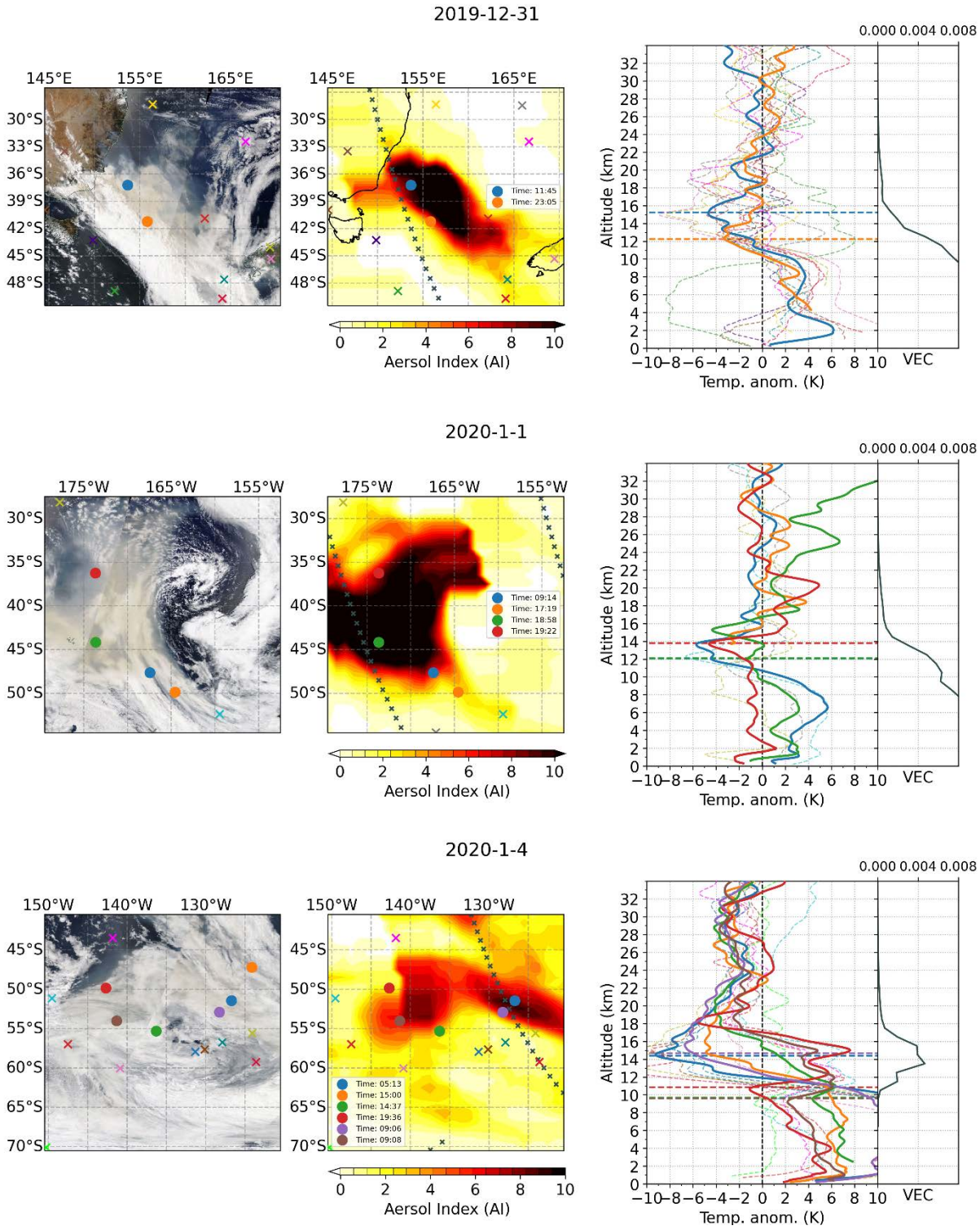

Figure 6: MODIS satelite image (left), Aerosol Index (AI) (center) and RO temperature profiles(right) as well as OMPS-LP aerosol data (VEC; right subpanel) for the examined area on Dec. 31, Jan. 1 and 4. Colored dots and x icons represent the locations for the RO-profiles inside and outside the aerosol plume, respectively. Black crosses in the central plot indicate the locations of the OMPS-LP measurements. Horizontal colored dashed lines in the right plots indicate the lapse rate tropopause for the individual profiles.

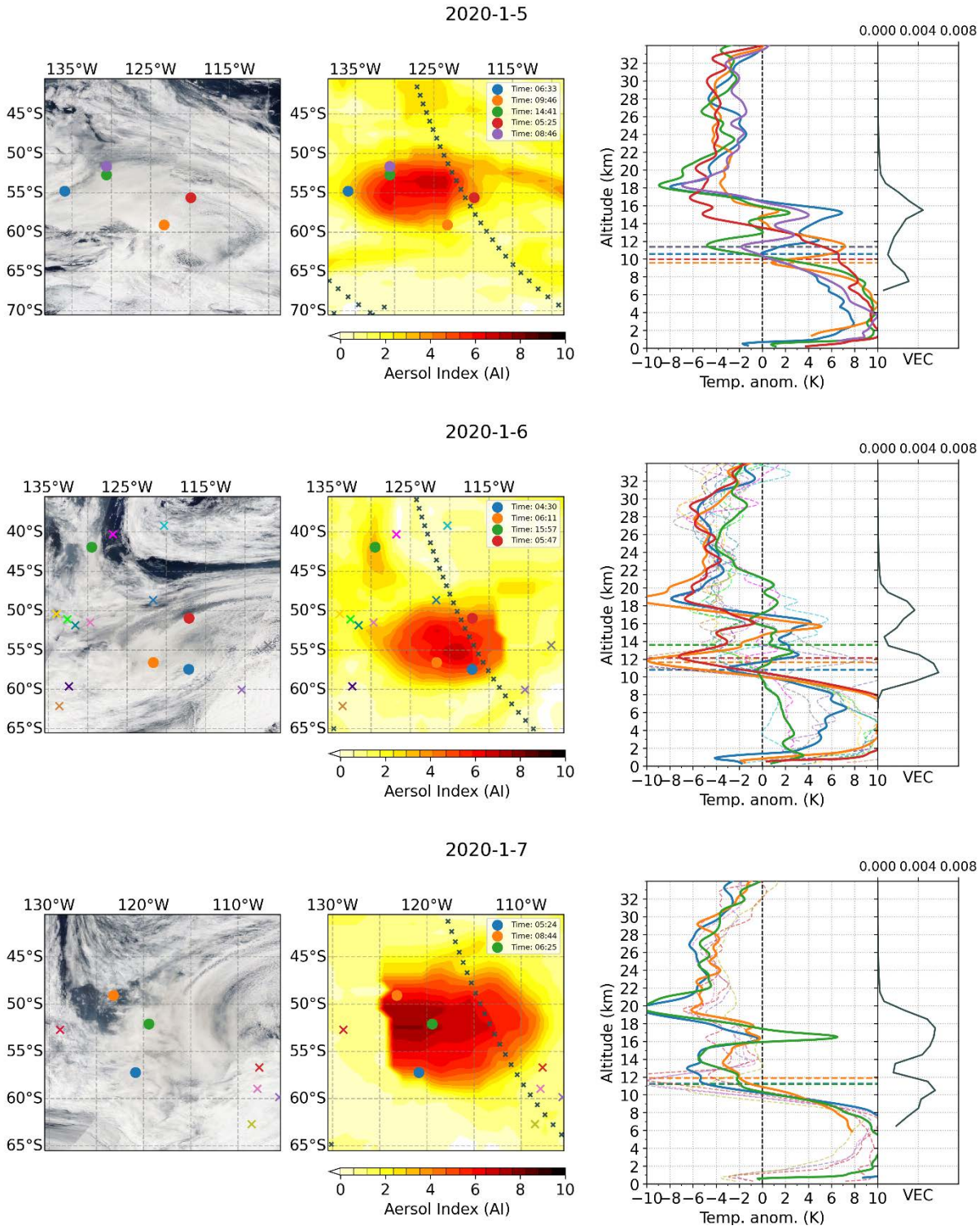

Figure 7: MODIS satelite image (left), Aerosol Index (AI) (center) and RO temperature profiles(right) as well as OMPS-LP aerosol data (VEC; right subpanel) for the examined area on Jan. 5, 6 and 7. Colored dots and x icons represent the locations for the RO-profiles inside and outside the aerosol plume, respectively. Black crosses in the central plot indicate the locations of the OMPS-LP measurements. Horizontal colored dashed lines in the right plots indicate the lapse rate tropopause for the individual profiles.

As the aerosol cloud is further transported to the east across the Pacific Ocean, a pronounced relative warming peak evolves in the lowermost stratosphere (Fig. 7). This relative warming is similar to the structure found for the 2017 Northern American wildfire event, yet far more pronounced. Additionally, OMPS-LP aerosol data are highly elevated at lower stratospheric altitudes, indicating the presence of wildfire aerosols. While a part of the aerosol cloud is quickly transported further to the east another part of the cloud moves eastwards at a slower pace (Fig. 7, top). The slower moving part forms an aerosol vortex which is clearly visible in the AI map (Fig. 7, middle and bottom) and has been investigated by Khaykin et al. (2020). The profiles co-located with the vortex show extreme warming peaks about 10 K in the lower stratosphere while the faster moving part of the aerosol cloud does not show a pronounced stratospheric warming (Fig. 6 bottom). Additionally, on Jan. 4 a second major pCb outbreak formed a massive aerosol plume which was transported eastwards (not shown).

On Jan.11 the aerosol cloud already reached an altitude of ~20 km. While RO profiles co-located with the vortex show a pronounced spike at this altitude, profiles outside the central region of the vortex also exhibit a strong warming, which extends from the tropopause up to the top of the vortex. In addition, the AI outside of the central vortex is also elevated, indicating that at the wildfire aerosols have already been distributed over a broad region in the stratosphere.

In the following days, pronounced warming of the whole lower stratosphere is clearly observed with RO (Fig. 8), while Khaykin et al. (2020) could only observe a warming within a confined altitude region. This can be explained by the fact that they analyzed deviations from a 3-day mean temperature, while in this study we analyzed temperature anomalies relative to the long-term monthly mean temperature.

Above the maximum warming, the RO profiles also show a cooling of the local stratosphere (Fig. 7), strongest within the vortex. This reflects the dipole structure described by Khaykin et al. (2020).

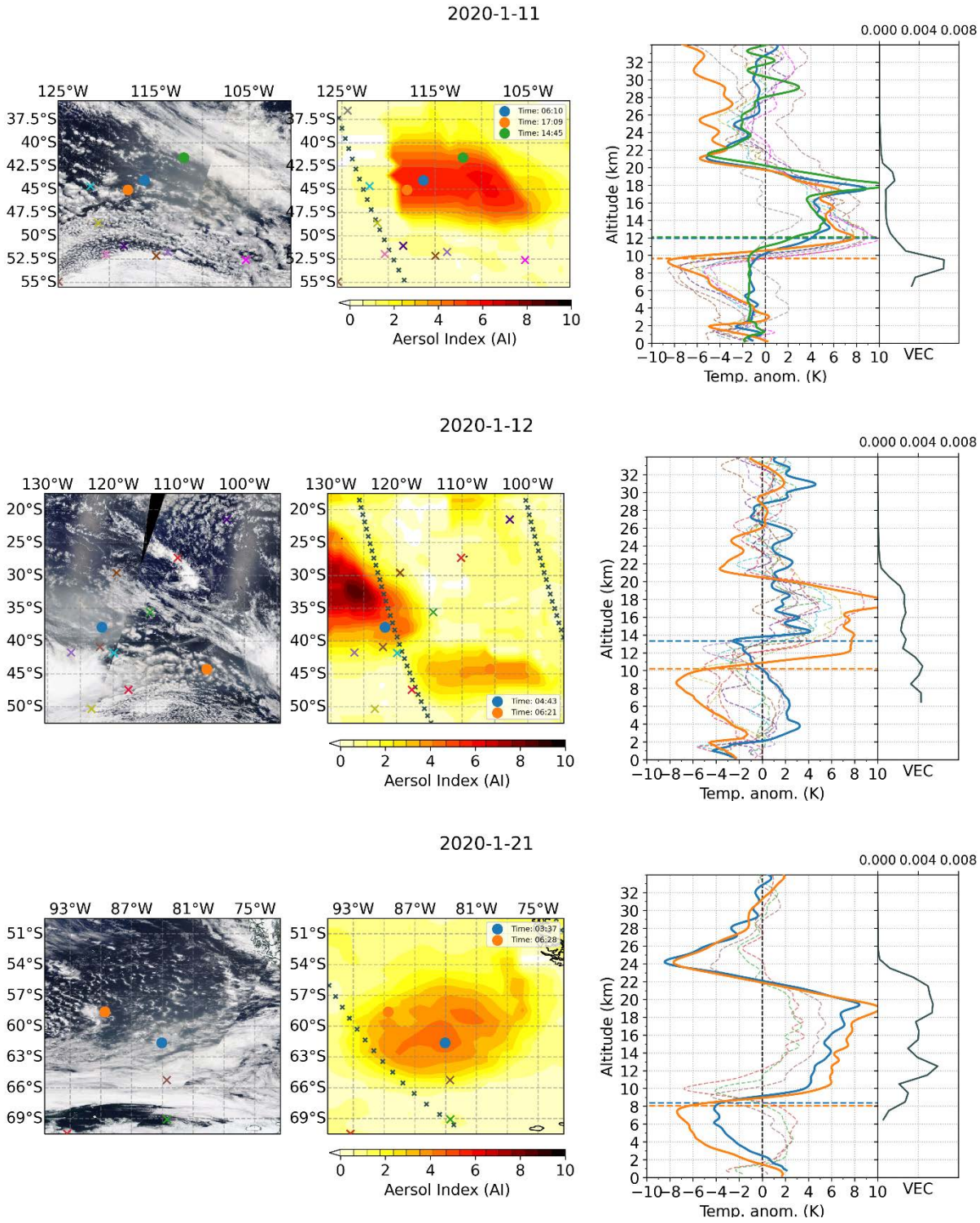

Figure 8: MODIS satelite image (left), Aerosol Index (AI) (center) and RO temperature profiles(right) as well as OMPS-LP aerosol data (VEC; right subpanel) for the examined area on Jan. 11, 12 and 21. Colored dots and x icons represent the locations for the RO-profiles inside and outside the aerosol plume, respectively. Black crosses in the central plot indicate the locations of the OMPS-LP measurements. Horizontal colored dashed lines in the right plots indicate the lapse rate tropopause for the individual profiles.

The massive aerosol plume originating from the second pCb outbreak passes the vortex area on Jan. 12 (Fig. 8). RO profiles co-located with this second cloud, however, do not show a warming in the lower stratosphere which suggests that this second outbreak did not strongly affect the stratosphere (e.g., Fig. 8 bottom).

Fig. 9 and Fig. 10 display the altitude evolution of the aerosol vortex which rises from 18 km on Jan. 4 to 24 km on Jan. 22, also shown in cloud top heights from RO and OMPS-LP aerosol measurements (Fig. 11). The strong uplift is regarded to be mainly caused by the strong heating potential of the wildfire aerosols which contain high amounts of black carbon. Compared to volcanic plumes, such a fast vertical movement through convection is exceptional since in the stratosphere volcanic plumes rise only a few kilometers within a matter of months and, at least in the tropics, this vertical motion is mainly driven by the stratospheric circulation.

Note that only a selection of plots for the period studied are shown in this section. The complete set of plots can be found in the appendix (Sect. A and Sect. B).

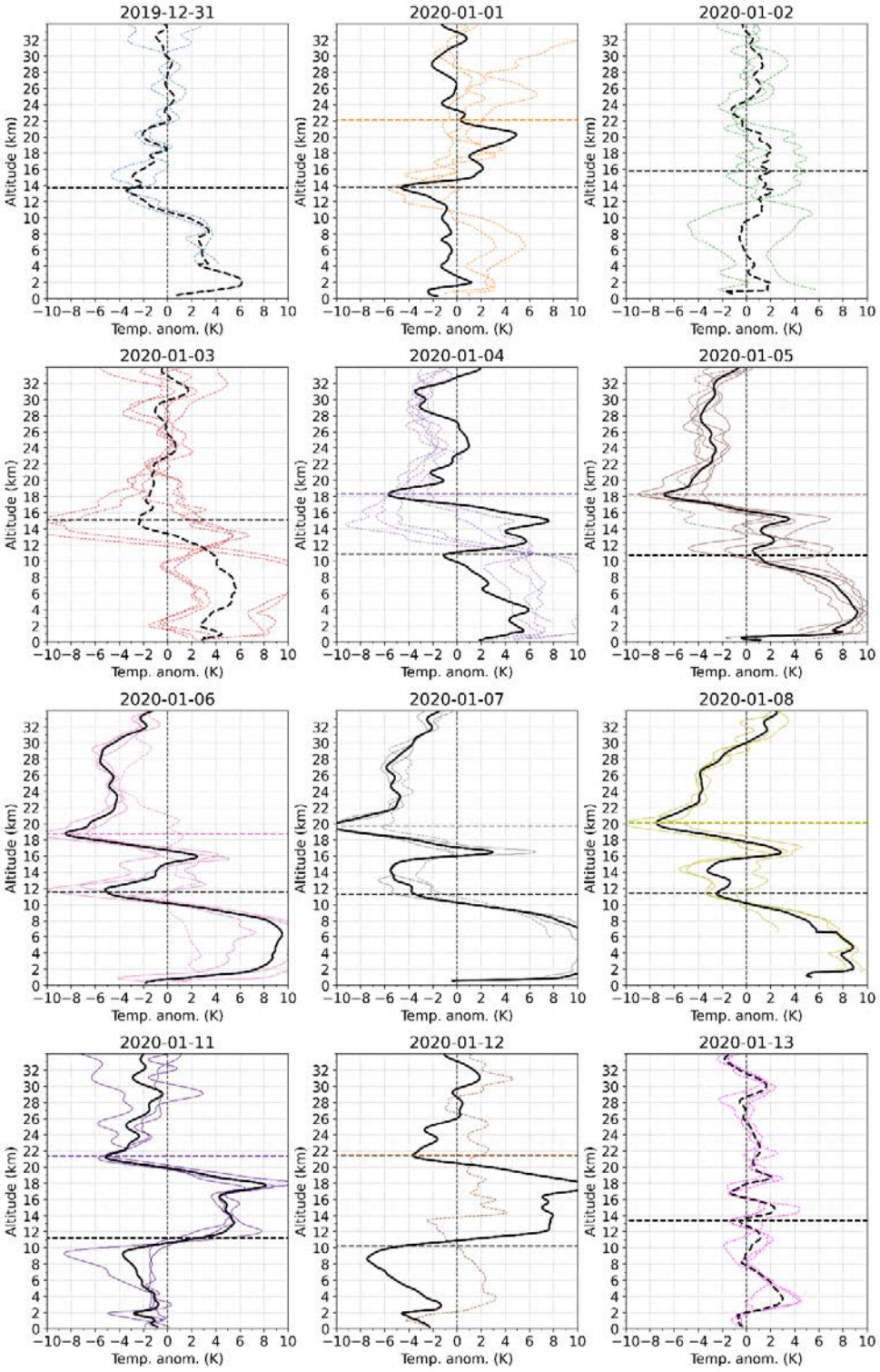

Figure 9: RO temperature profiles within the wildfire aerosol cloud (colored) and the mean temperature profile (black) for each day for 31 Dec. 2019 – 13 Jan. 2020. The color-code refers to the different regions examined on the individual days (see Fig. 5). The horizontal black dashed line denotes the mean lapse rate tropopause while the colored dashed horizontal line denotes the estimated plume top altitude. Profiles which do not show a peak exceeding 3 K are dashed and were not considered for the calculation of the mean value.

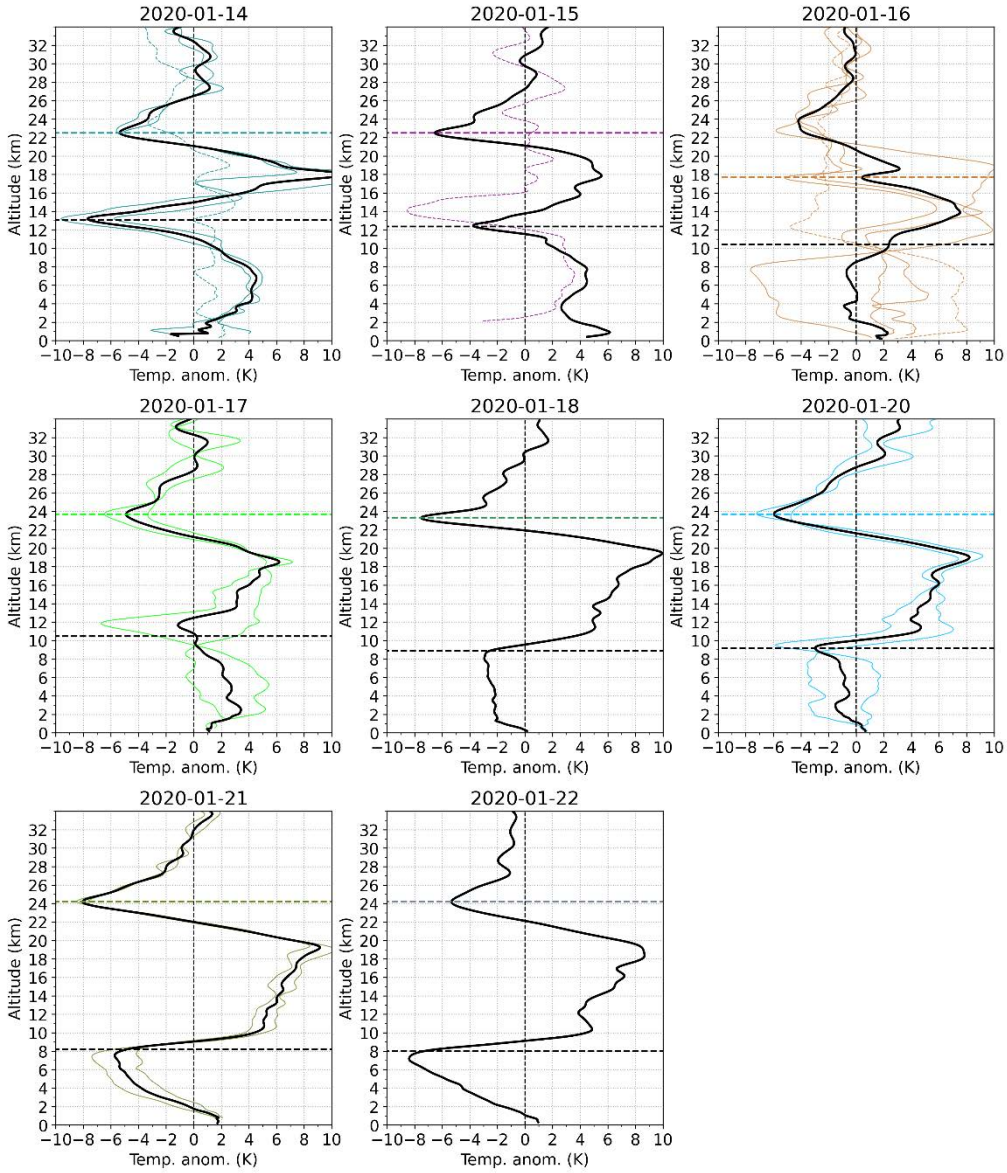

Figure 10: RO temperature profiles within the wildfire aerosol cloud (colored) and the mean temperature profile (black) for each day for 14–22 Jan. 2020. The color-code refers to the different regions examined on the individual days (see Fig. 5). The horizontal black dashed line denotes the mean lapse rate tropopause while the colored dashed horizontal line denotes the estimated plume top altitude. Profiles which do not show a peak exceeding 3 K are dashed and were not considered for the calculation of the mean value.

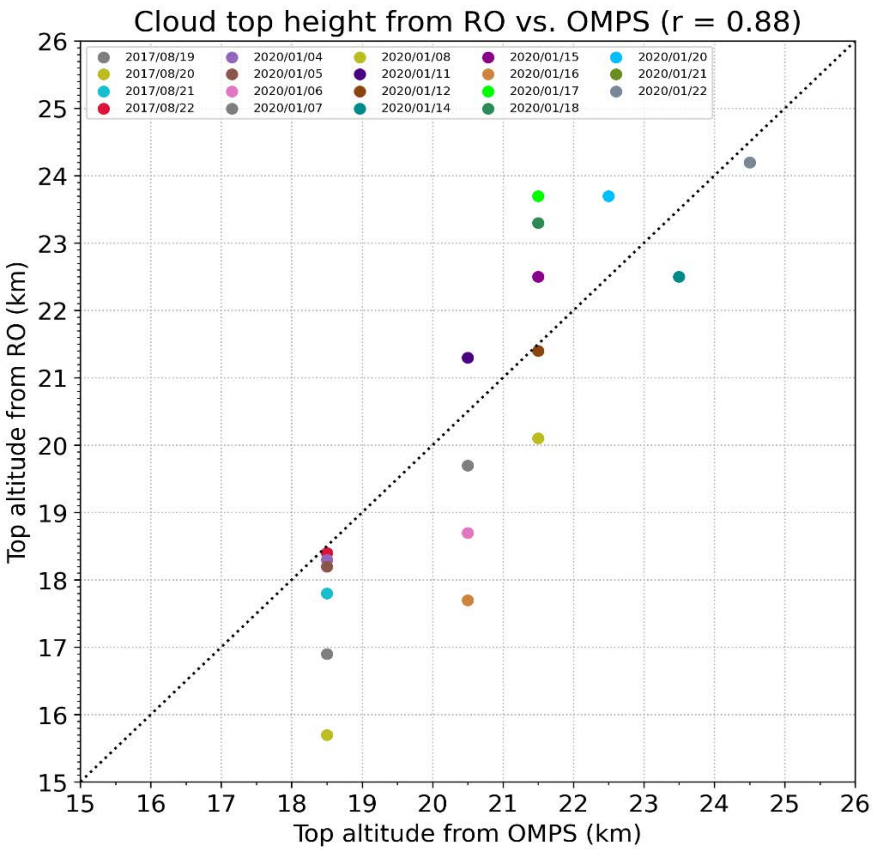

Figure 11: Correlation between the cloud top altitude derived from the RO temperature measurements and OMPS-LP aerosol measurements for the 2017 Northern American and 2019/20 Australian wildfires. Jan.1, 2020 is excluded since it is not clear whether the peak in the RO data is associated with wildfire aerosols.

3.2. Short-term climate imprints from wildfires compared to volcanic climate signals

In addition to the temporal evolution of the wildfire plumes, the impact of intense wildfires on the short-term climate in the upper troposphere lower stratosphere was investigated with RO gridded records. Therefore, the mean temperature anomalies (averaged over three months) before the event are compared to the mean temperature anomalies (averaged over three months) after the start of the event.

The stratospheric climate signals of the 2017 Northern American wildfires and the 2020 Australian wildfires are analyzed and set into context with signals of volcanic eruptions. The Calbuco eruption in 2015 was one of the largest eruptions since the Pinatubo in 1991 and is investigated using the same approach. Please note the different color bars used for the plots when comparing the results.

3.2.1. Northern American wildfires 2017

The GloSSAC aerosol extinction perturbation for the 2017 Northern American wildfires (Fig. 12 left) shows two pronounced peaks, one directly above the tropopause at high latitudes and another one at mid latitudes between 40°N and 50°N. The high-latitude perturbation is accompanied by a comparatively small warming signal directly above the tropopause, visible in the RO data (Fig. 12 right). While the aerosol extinction perturbation at mid latitudes is less pronounced than the high latitude peak the associated warming signal observed with RO is more intense with a magnitude of up to 1 K. This behavior has already been described by Stocker et al. (2019) and Mehta et al. (2015) who observed the warming signals for volcanic eruptions. They found that the warming in general is stronger the closer to the equator. The findings are also in line with the temperature profiles shown in Sect. 3.1.1, where the strongest lower tropospheric warming is observed as the aerosol cloud crosses the Atlantic Ocean at mid latitudes.

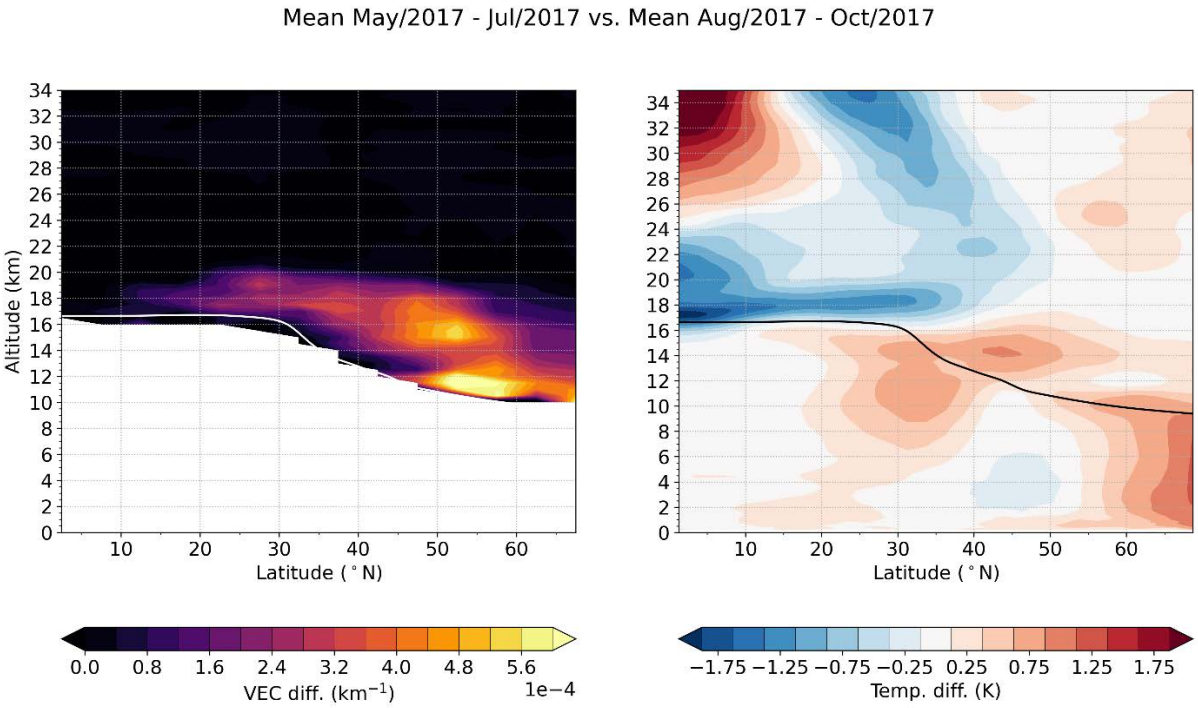

Figure 12: Difference in the mean GloSSAC aerosol concentration (VEC) three months before the 2017 Northern American wildfire event vs. three months after the event (left) as well as the corresponding difference in the RO temperature.

3.2.2. Calbuco eruption 2015

The stratospheric temperature imprints of post-2000 volcanic eruptions were investigated by Stocker et al. (2019). They found that the Calbuco eruption had been the strongest eruption in the southern mid-latitudes during the last 20 years in terms of the temperature imprint.

The aerosol extinction anomaly three months before the eruption compared to three months after the eruption shows a strong signal between 60°S and 10°S peaking at ~35°S. Depending on the latitude the signal extends from the tropopause up to 20 km. The corresponding differences in the RO temperature anomalies show a warming of 0.5 K in the lower stratosphere between 20°S and 10°S which agrees with the strong low latitude warming signal shown by Stocker et al. (2019). While the aerosol extinction anomaly from the Calbuco eruption is far more pronounced compared to the 2017 wildfire event, the temperature signals are comparable in magnitude, indicating a stronger heating potential of biomass burning aerosols compared to volcanic sulfate aerosols.

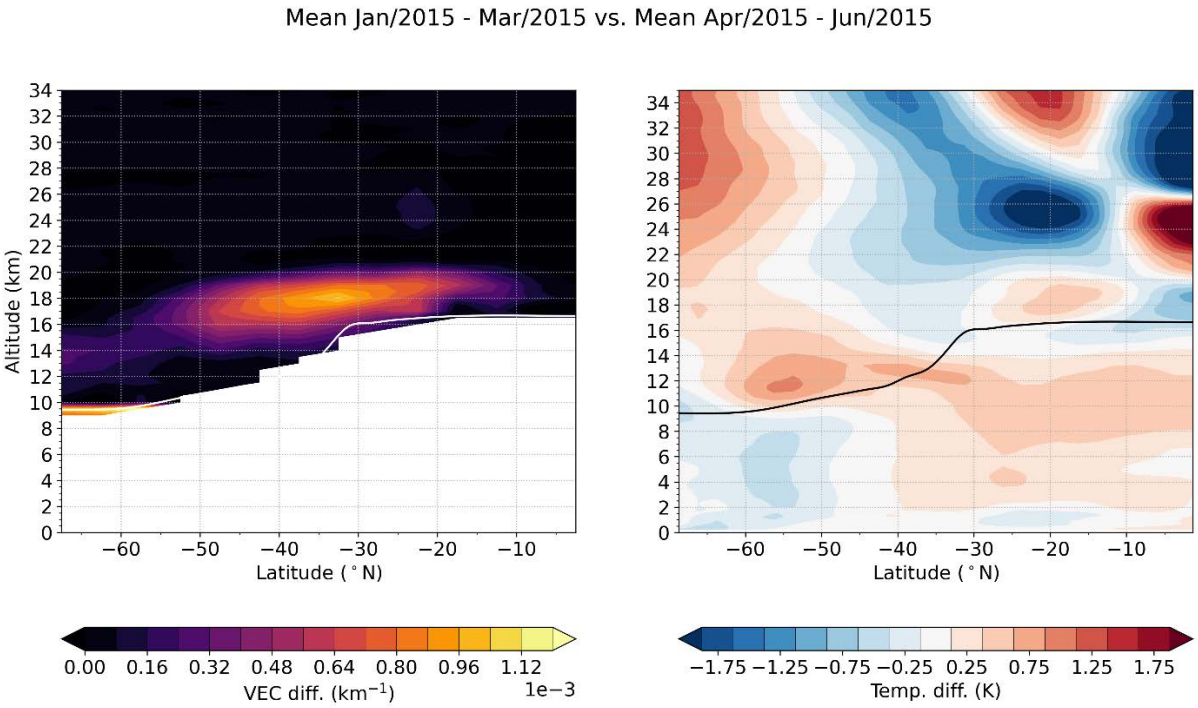

Figure 13: Difference in the mean GloSSAC aerosol concentration (VEC) three months before the 2015 Calbuco eruption vs. three months after the eruption (left) as well as the corresponding difference in the RO temperature.

3.2.3. Australian wildfires 2019/20

For the time of the 2019/20 wildfire event, there are no high resolution GloSSAC aerosol data available. However, Khaykin et al. (2020) compared the distortion in the Stratospheric Aerosol Optical Depth

(SAOD) from the 2019/20 Australian wildfires with those of the Calbuco eruption and the Northern American wildfires in 2017, respectively (see Khaykin et al., 2020, Fig. 3). They found that the disruption in the SAOD (which is the VEC summarized from the tropopause to the top of the atmosphere) caused by the Australian fires was comparable to the SAOD anomaly caused by the Calbuco eruption and three times as strong as the SAOD anomaly caused by the Northern American wildfires.

Fig. 14 displays the temperature signal associated with the 2019/20 Australian wildfires, and reveals distinct warming of the lower stratosphere. The warming in the lower stratosphere is strongest at mid latitudes around 35°S and reaches up to 3.5 K. This is more than three times the maximum warming caused by the 2017 Northern American wildfires and more than six times the maximum warming caused by the Calbuco eruption. This impressively shows the extensive heating potential of wildfire aerosols.

The stratospheric warming did not stop in March 2020 however, gridded RO data are currently only available until this date. A full characterization of this large stratospheric heating will be possible when RO data are processed at least until August or September 2020. However, so far, the observations indicate that this warming is potentially the strongest stratospheric temperature perturbation caused by aerosols since the eruption of the Pinatubo in 1991.

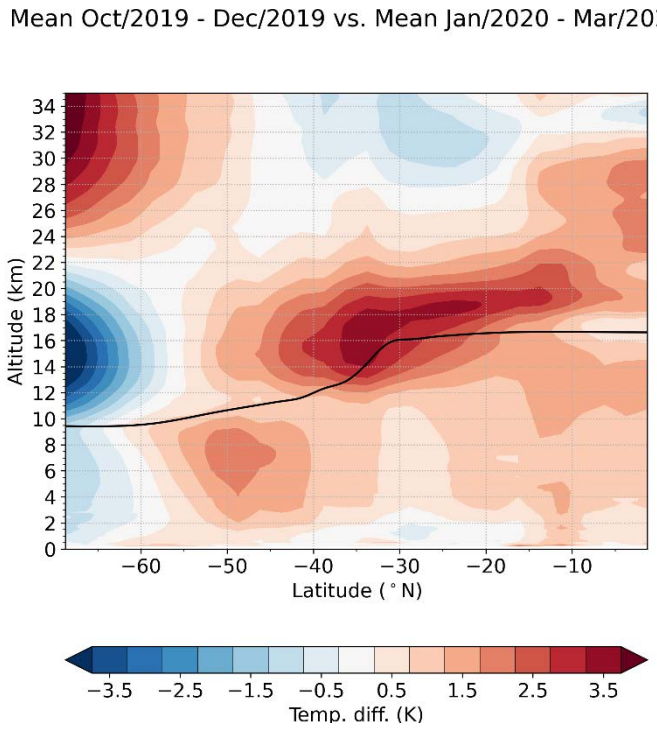

Figure 14: Difference in the monthly mean RO temperature anomalies three months before the 2020 Australian wildfire event vs. three months after the event.

4. Discussion and outlook

In this study, the effects of two major wildfire events on the vertical atmospheric temperature structure were investigated. For both, the Northern American wildfires in 2017 as well as the Australian wildfires in 2019/20, strong warming signals of up to 10 K were observed in the lower stratosphere in daily RO profiles located within the aerosol plumes. The aerosol clouds for both events were found to rise several kilometers in the stratosphere in just a few days. The top altitudes of the aerosol clouds were determined between 16 km and 24 km from the RO temperature data and found in good agreement with the top altitudes derived from aerosol measurements, proving the applicability of RO in this context.

Beside the daily evolution of the wildfire plumes, the climate signals of the events were investigated and compared to climate imprints of the Calbuco eruption in 2015. The results indicate a larger warming potential from wildfire aerosols compared to volcanic sulfate aerosols. For the Northern American wildfires the estimated impact was a lower stratospheric warming of 1 K, derived from the temperature before and after the event. For the Australian wildfires a warming of up to 3.5 K was estimated. The results suggest that the signal from the Australian wildfires is the strongest short-term climate imprint caused by aerosols since the Pinatubo eruption in 1991. Atmospheric variability modes apart from the seasonal cycle were not investigated as they are considered of minor relevance for the studied cases.

The results also suggest that wildfire signals, similar to volcanic signals (Stocker, et al., 2019), should not be neglected in climate trend studies concerning the lower stratosphere. While volcanic eruptions occur irregularly and cannot be influenced by human action, the risk of wildfires increases due to climate change (Flannigan et al., 2013; Langmann et al., 2009). Therefore, the impact of wildfires is expected to become increasingly important, especially for studies addressing the lower stratosphere.

Further investigation of more recent wildfires will help to clarify whether the 2019/20 Australian wildfires were an exception. However, as has been shown, also fires on the scale of the 2017 Northern American wildfires or even 2009 Bushfires (Siddaway & Petelina, 2011; Stocker, 2020) have the potential to cause substantial stratospheric perturbations, which can affect temperature trend detection.

RO data were found beneficial for investigating wildfires with the potential to affect stratospheric temperatures. The results also prove that the RO data are suited to create a spatially and temporally high resolved gridded data set, which can be used to generate new insights into regional temperature imprints from particularly large wildfires. A temporal resolution of days is required, and provided by RO, due to the very high dynamic of the aerosol plumes in their horizontal and vertical evolution.

Overall, the results show that closer investigation of wildfire events using RO measurements can significantly improve our knowledge about wildfire plume dynamics and will be beneficial to reduce remaining uncertainties, especially in stratospheric temperature trend detection.

References

Angerer, B., Ladstädter, F., Scherllin-Pirscher, B., Schwärz, M., Steiner, A. K., Foelsche, U., & Kirchengast, G. (2017). Quality aspects of the Wegener Center multi-satellite GPS radio occultation record OPSv5.6. *Atmospheric Measurement Techniques, 10*, 4845–4863. doi:10.5194/amt-10-4845-2017

Ansmann, A., Baars, H., Chudnovsky, A., Mattis, I., Veselovskii, I., Haarig, M., . . . Wandinger, U. (2018). Extreme levels of Canadian wildfire smoke in the stratosphere over central Europe on 21–22 August 2017. *Atmospheric Chemistry and Physics, 18*, 11831–11845. doi:10.5194/acp-18-11831-2018

Anthes, R. A. (2011). Exploring Earth's atmosphere with radio occultation: contributions to weather, climate and space weather. *Atmospheric Measurement Techniques, 4*, 1077–1103. doi:10.5194/amt-4-1077-2011

Biondi, R., Ho, S.-P., Randel, W., Syndergaard, S., & Neubert, T. (2013). Tropical cyclone cloud-top height and vertical temperature structure detection using GPS radio occultation measurements. *Journal of Geophysical Research: Atmospheres, 118*, 5247-5259. doi:10.1002/jgrd.50448

Biondi, R., Steiner, A. K., Kirchengast, G., Brenot, H., & Rieckh, T. (2017). Supporting the detection and monitoring of volcanic clouds: A promising new application of Global Navigation Satellite System radio occultation. *Advances in Space Research, 60*, 2707-2722. doi:10.1016/j.asr.2017.06.039

EOPAC Team. (2019). *Wegener Center GNSS radio occultation record OPS 5.6 2001–2018.* University of Graz, Austria, doi:10.25364/WEGC/OPS5.6:2019.1

Flannigan, M., Cantin, A. S., de Groot, W. J., Wotton, M., Newbery, A., & Gowman, L. M. (2013). Global wildland fire season severity in the 21st century. *Forest Ecology and Management, 294*, 54-61. doi:https://doi.org/10.1016/j.foreco.2012.10.022

Fromm, M., Lindsey, D. T., Servranckx, R., Yue, G., Trickl, T., Sica, R., . . . Godin-Beekmann, S. (2010). The Untold Story of Pyrocumulonimbus. *Bulletin of the American Meteorological Society, 91*, 1193-1210. doi:10.1175/2010BAMS3004.1

Hammer, M. S., Martin, R. V., van Donkelaar, A., Buchard, V., Torres, O., Ridley, D. A., & Spurr, R. J. (2016). Interpreting the ultraviolet aerosol index observed with the OMI satellite instrument to understand absorption by organic aerosols: implications for atmospheric oxidation and direct radiative effects. *Atmospheric Chemistry and Physics, 16*, 2507–2523. doi:10.5194/acp-16-2507-2016

Johnston, B. R., Xie, F., & Liu, C. (2018). The Effects of Deep Convection on Regional Temperature Structure in the Tropical Upper Troposphere and Lower Stratosphere. *Journal of Geophysical Research: Atmospheres, 123*, 1585-1603. doi:https://doi.org/10.1002/2017JD027120

Khaykin, S., Legras, B., Bucci, S., Sellitto, P., Isaksen, L., Tencé, F., . . . Godin-Beekmann, S. (2020). The 2019/20 Australian wildfires generated a persistent smoke-charged vortex rising up to 35 km altitude. *Communications Earth & Environment, 1*, 22. doi:10.1038/s43247-020-00022-5

Kovilakam, M., Thomason, L., Ernest, N., Rieger, L., Bourassa, A., & Millán, L. (2020). A Global Space-based Stratospheric Aerosol Climatology (Version 2.0): 1979–2018. *Earth System Science Data Discussions, 2020*, 1–41. doi:10.5194/essd-2020-56

Langmann, B., Duncan, B., Textor, C., Trentmann, J., & van der Werf, G. R. (2009). Vegetation fire emissions and their impact on air pollution and climate. *Atmospheric Environment, 43*, 107-116. doi:https://doi.org/10.1016/j.atmosenv.2008.09.047

Liu, N., & Liu, C. (2016). Global distribution of deep convection reaching tropopause in 1 year GPM observations. *Journal of Geophysical Research: Atmospheres, 121*, 3824-3842. doi:https://doi.org/10.1002/2015JD024430

Mehta, S. K., Fujiwara, M., Tsuda, T., & Vernier, J.-P. (2015). Effect of recent minor volcanic eruptions on temperatures in the upper troposphere and lower stratosphere. *Journal of Atmospheric and Solar-Terrestrial Physics, 129*, 99-110. doi:https://doi.org/10.1016/j.jastp.2015.04.009

Paugam, R., Wooster, M., Freitas, S., & Val Martin, M. (2016). A review of approaches to estimate wildfire plume injection height within large-scale atmospheric chemical transport models. *Atmospheric Chemistry and Physics, 16*, 907–925. doi:10.5194/acp-16-907-2016

Peterson, D. A., Campbell, J. R., Hyer, E. J., Fromm, M. D., Kablick, G. P., Cossuth, J. H., & DeLand, M. T. (2018). Wildfire-driven thunderstorms cause a volcano-like stratospheric injection of smoke. *npj Climate and Atmospheric Science, 1*, 30. doi:10.1038/s41612-018-0039-3

Schwärz, M., Kirchengast, G., Scherllin-Pirscher, B., Schwarz, J., Ladstädter, F., & Angerer, B. (2016). *Multi-Mission Validation by Satellite RadioOccultation Extension Project - Final Report.* Tech. Rep. for ESA⁄ESRIN No. 01/2016, Wegener Center, University of Graz, Graz, Austria. Available from: https://wegcwww.uni-graz.at/publ/wegcpubl/arsclisys/2016/Schwaerz-etal_MMValRO-FinRep_Dec2016.pdf

Siddaway, J. M., & Petelina, S. V. (2011). Transport and evolution of the 2009 Australian Black Saturday bushfire smoke in the lower stratosphere observed by OSIRIS on Odin. *Journal of Geophysical Research: Atmospheres, 116*. doi:https://doi.org/10.1029/2010JD015162

Steiner, A. K., Hunt, D., Ho, S.-P., Kirchengast, G., Mannucci, A. J., Scherllin-Pirscher, B., . . . Wickert, J. (2013). Quantification of structural uncertainty in climate data records from GPS radio occultation. *Atmospheric Chemistry and Physics, 13*, 1469–1484. doi:10.5194/acp-13-1469-2013

Steiner, A. K., Lackner, B. C., Ladstädter, F., Scherllin-Pirscher, B., Foelsche, U., & Kirchengast, G. (2011). GPS radio occultation for climate monitoring and change detection. *Radio Science, 46*. doi:10.1029/2010RS004614

Steiner, A. K., Ladstädter, F., Ao, C. O., Gleisner, H., Ho, S.-P., Hunt, D., . . . Wickert, J. (2020). Consistency and structural uncertainty of multi-mission GPS radio occultation records. *Atmospheric Measurement Techniques, 13*, 2547–2575. doi:10.5194/amt-13-2547-2020

Stocker, M. (2020). *Signals of recent volcanic eruptions in vertically resolved atmospheric temperature (Master thesis).* Wegener Center,. Graz, Austria: Wegener Center Verlag. Available from: https://wegcwww.uni-graz.at/publ/wegcreports/2020/WCV-SciRep-No86-MStocker-May2020.pdf

Stocker, M., Ladstädter, F., Wilhelmsen, H., & Steiner, A. K. (2019). Quantifying Stratospheric Temperature Signals and Climate Imprints From Post-2000 Volcanic Eruptions. *Geophysical Research Letters, 46*, 12486-12494. doi:10.1029/2019GL084396

Thomason, L. W., Ernest, N., Millán, L., Rieger, L., Bourassa, A., Vernier, J.-P., . . . Peter, T. (2018). A global space-based stratospheric aerosol Climatology: 1979–2016. *Earth System Science Data, 10*, 469–492. doi:10.5194/essd-10-469-2018

Torres, O. O. (2006). OMI/Aura Near UV Aerosol Optical Depth and Single Scattering Albedo 1-orbit L2 Swath 13x24 km V003. Goddard Earth Sciences Data and Information Services Center (GES DISC). doi:10.5067/Aura/OMI/DATA2004

Yu, P., Toon, O. B., Bardeen, C. G., Zhu, Y., Rosenlof, K. H., Portmann, R. W., . . . Robock, A. (2019). Black carbon lofts wildfire smoke high into the stratosphere to form a persistent plume. *Science, 365*, 587–590. doi:10.1126/science.aax1748

Zawada, D. J., Rieger, L. A., Bourassa, A. E., & Degenstein, D. A. (2018). Tomographic retrievals of ozone with the OMPS Limb Profiler: algorithm description and preliminary results. *Atmospheric Measurement Techniques, 11*, 2375–2393. doi:10.5194/amt-11-2375-2018

Appendix

A. Evolution of the 2017 Northern American wildfire plume (all days)

The following plots display the evolution of the 2017 Northern American wildfire plume from Aug.12, 2017 to Aug. 22, 2017.

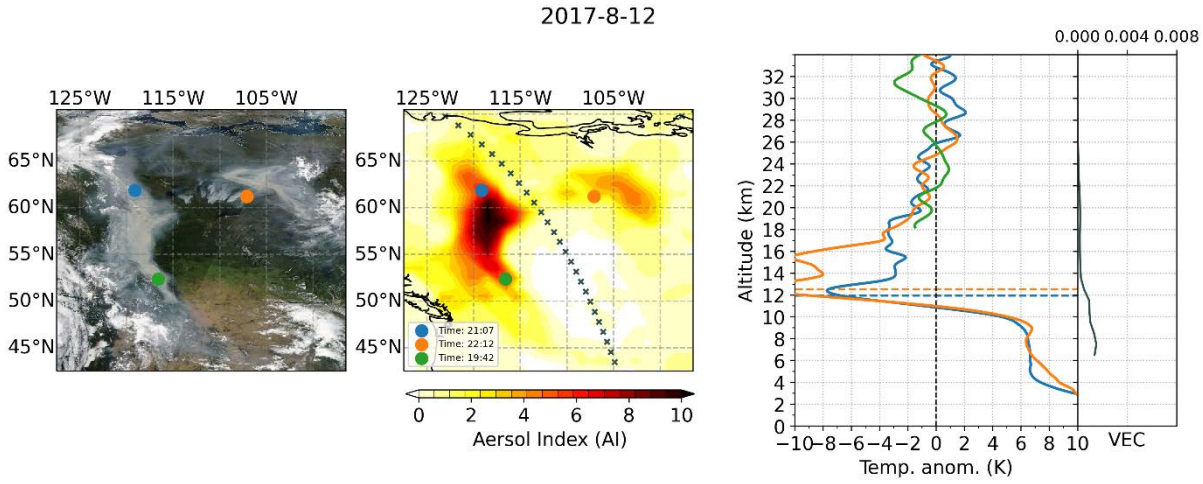

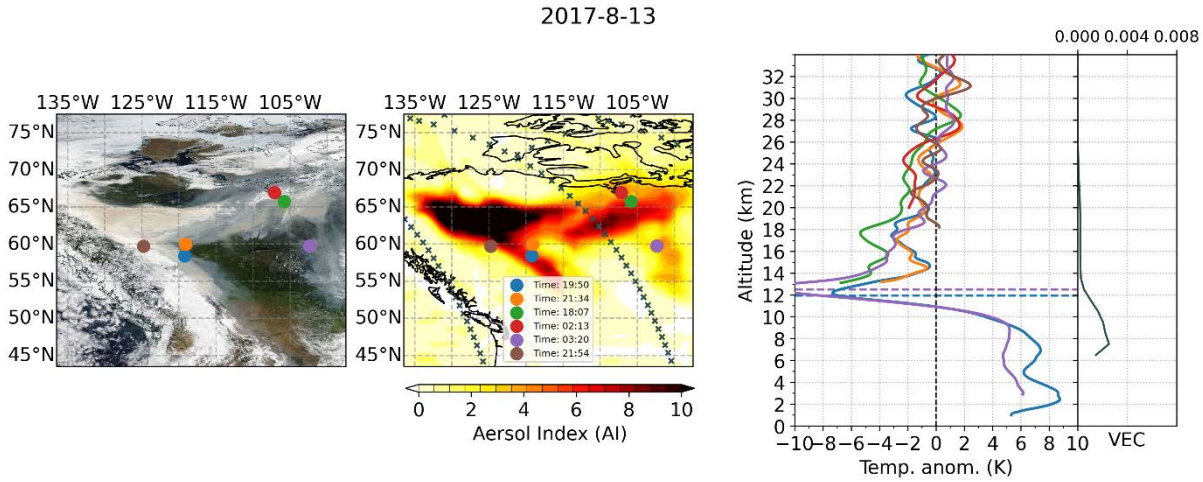

2017-8-14

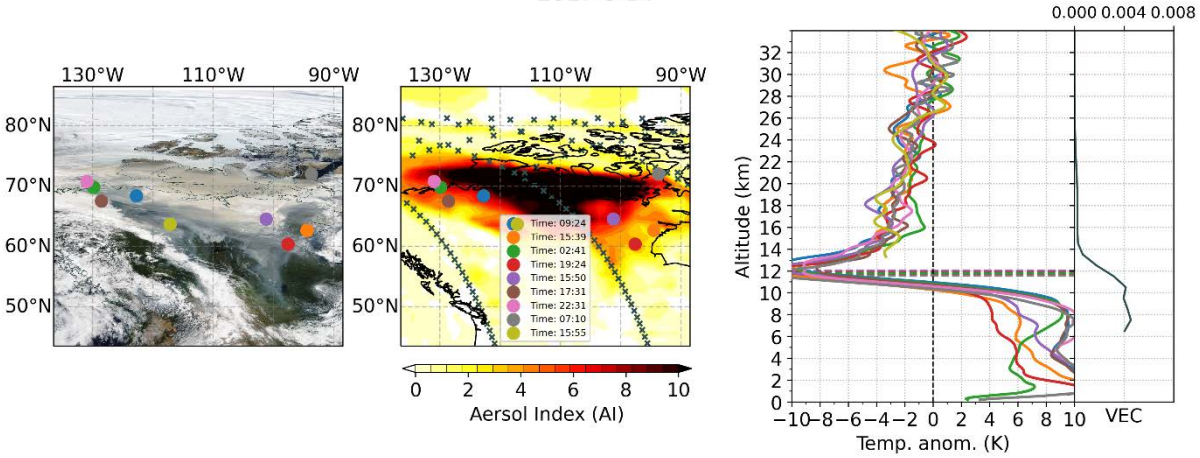

2017-8-15

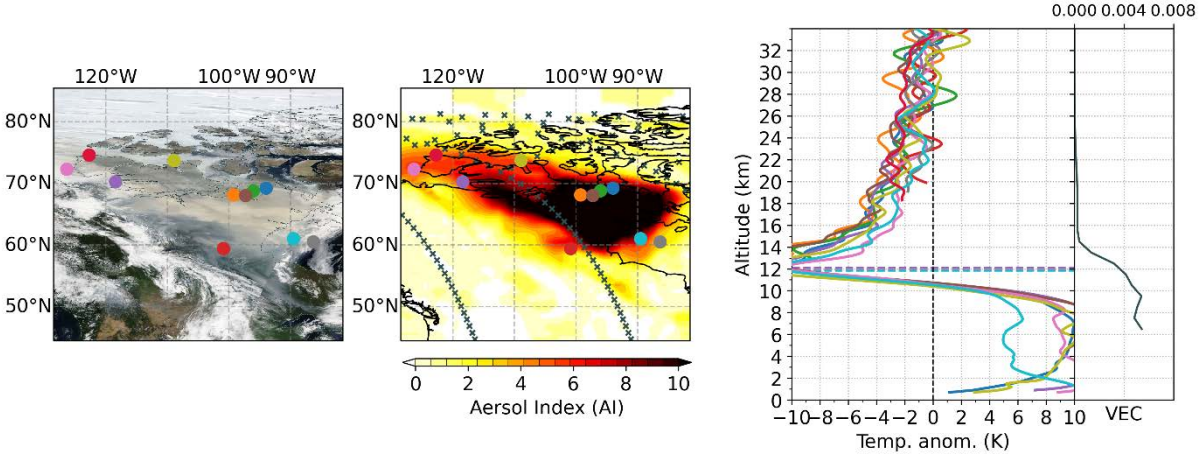

2017-8-16

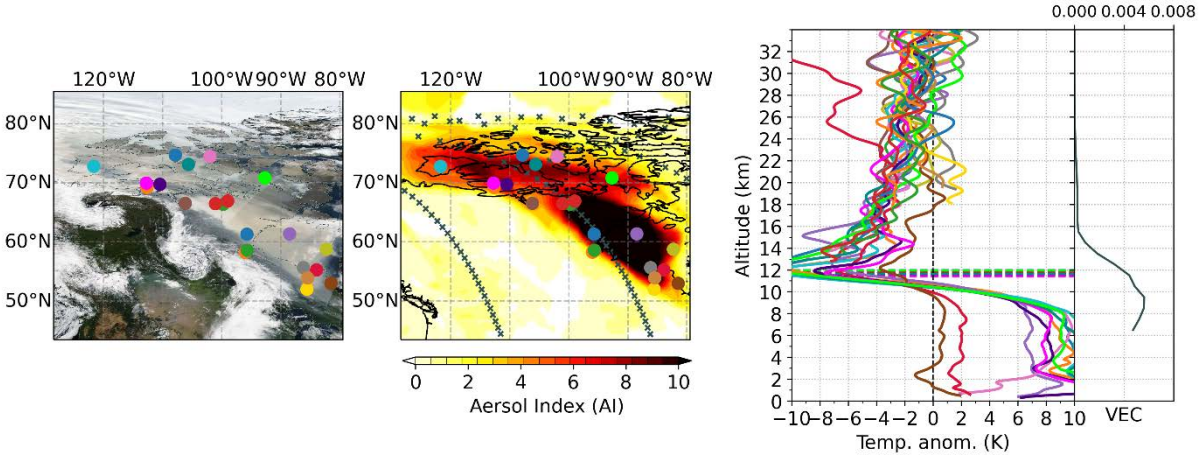

2017-8-17

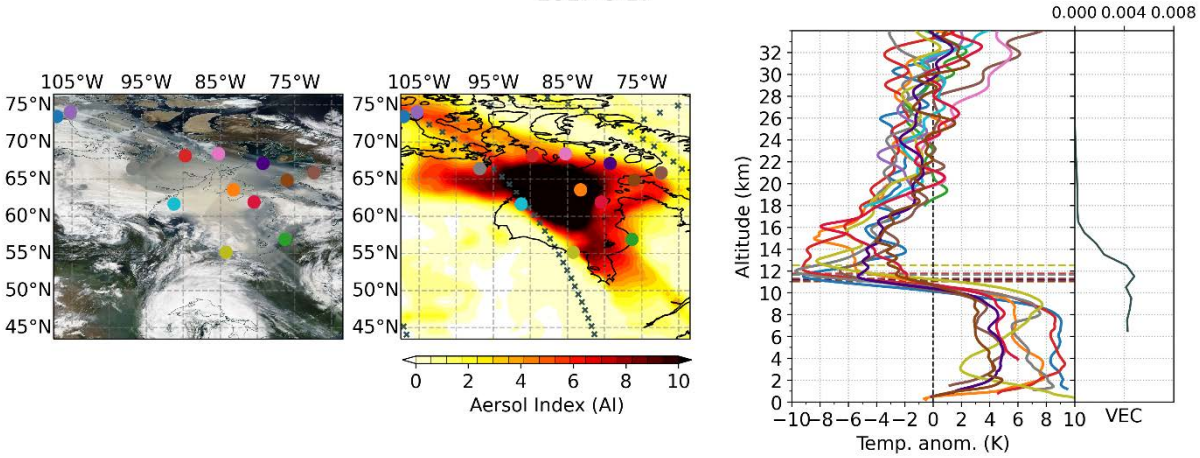

2017-8-18

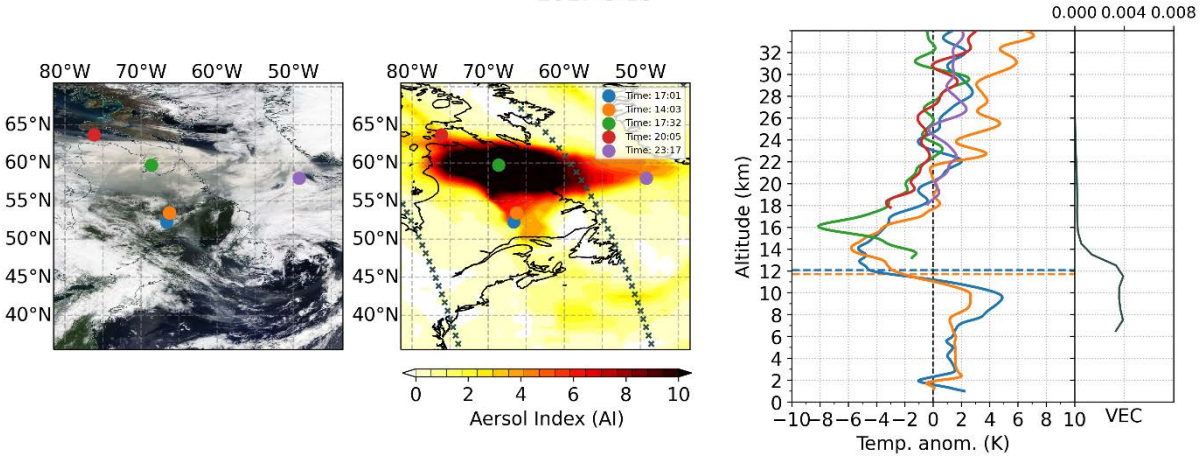

2017-8-19

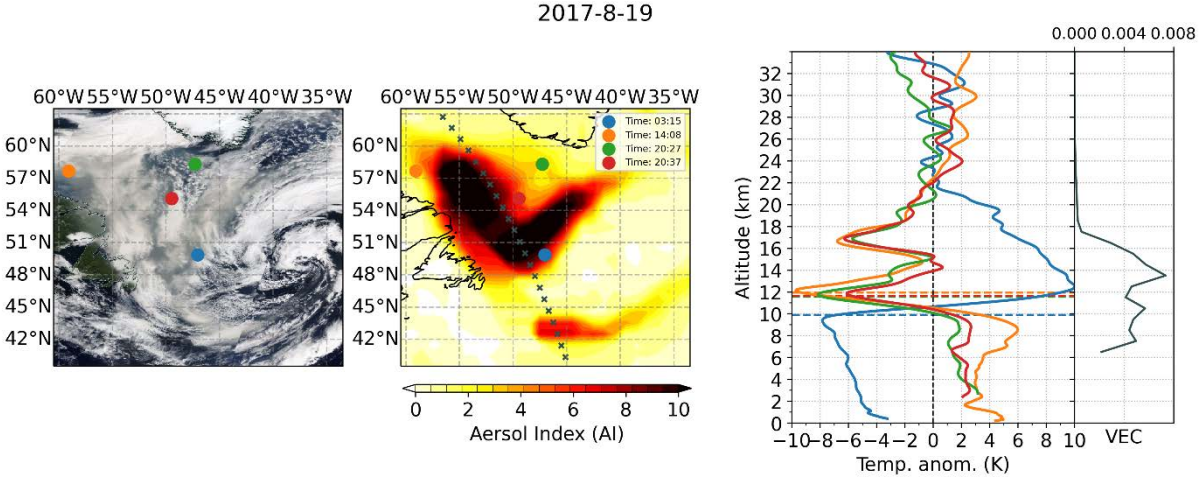

2017-8-20

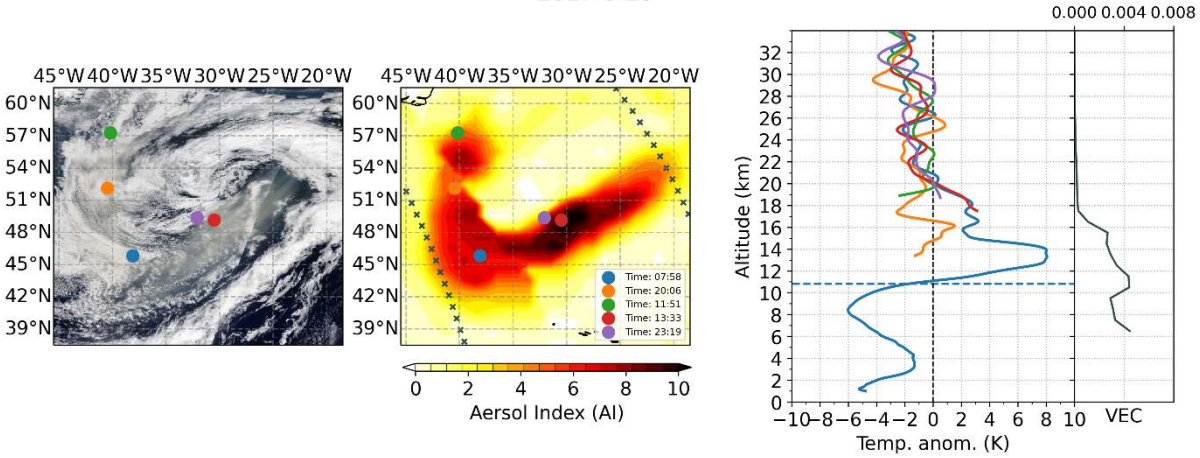

2017-8-21

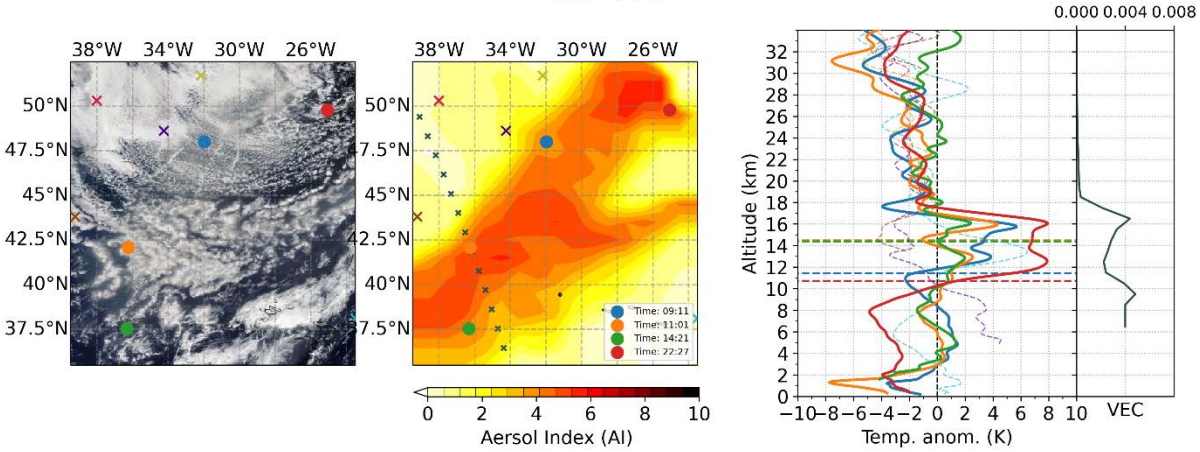

2017-8-22

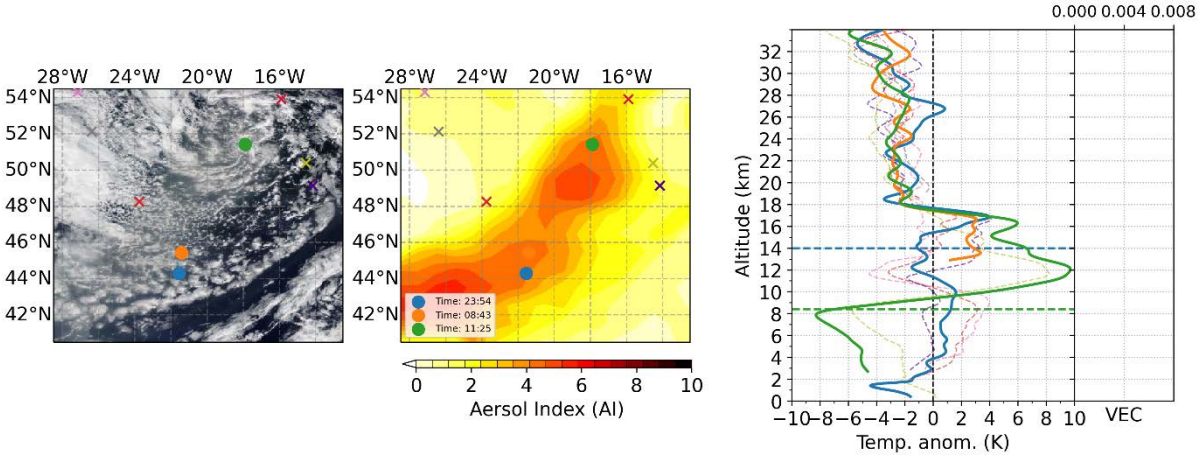

B. Evolution of the 2017 Northern American wildfire plume (all days)

The following plots display the evolution of the 2017 Northern American wildfire plume from Dec. 31, 2019 to Jan. 22, 2020.

2019-12-31

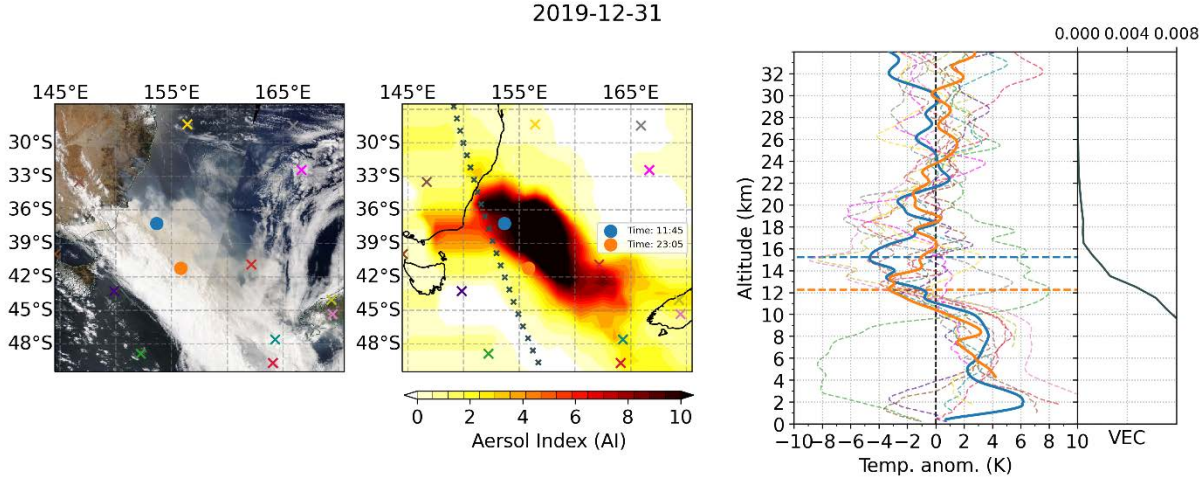

2020-1-1

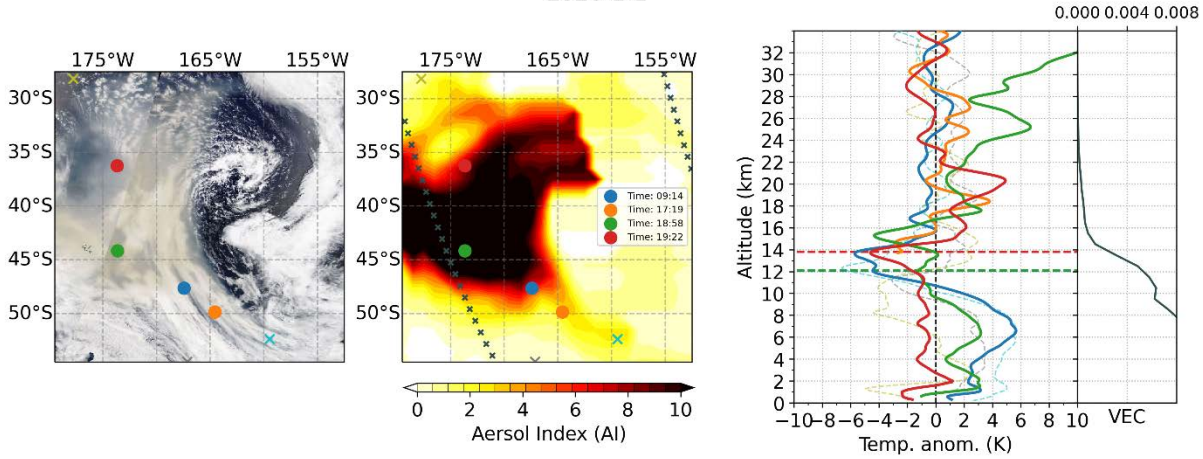

2020-1-2

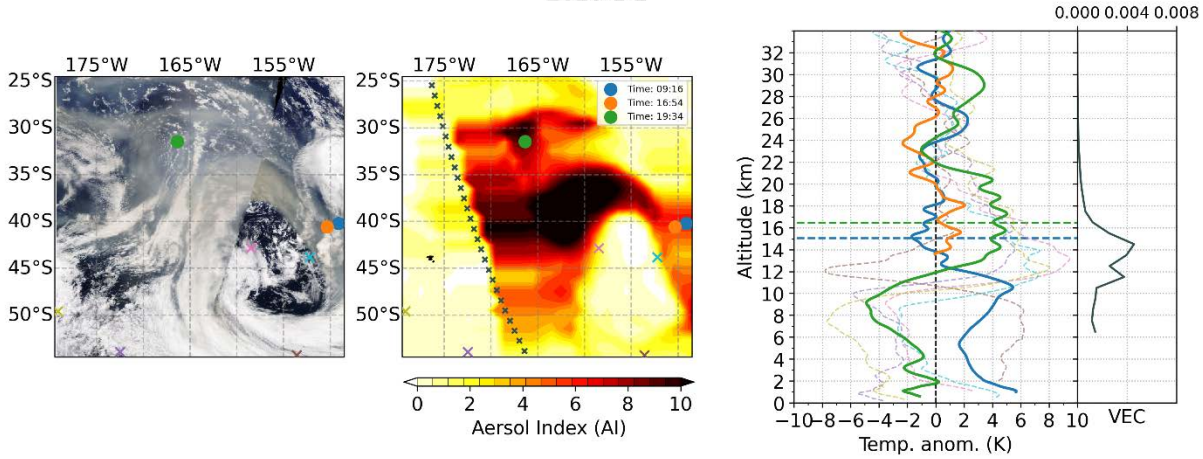

2020-1-3

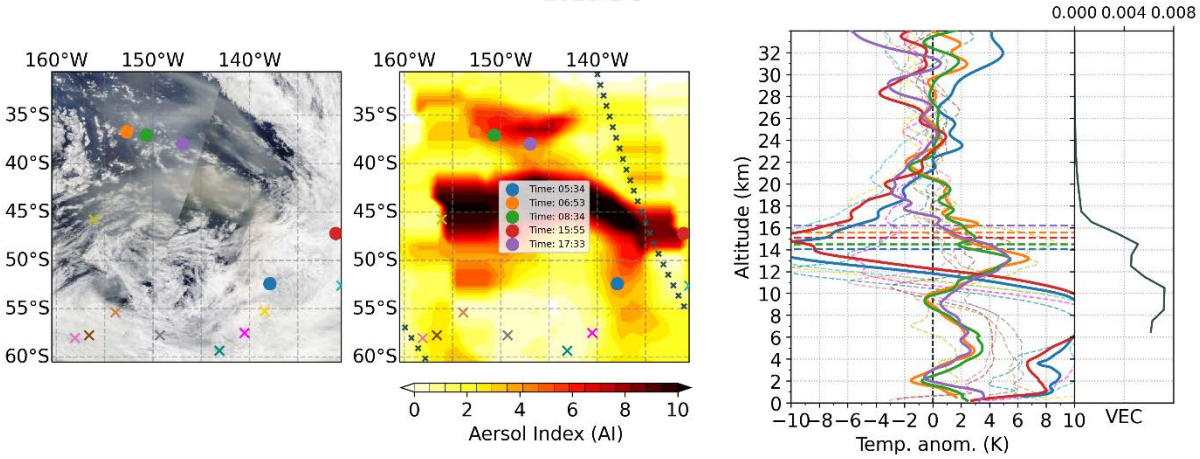

2020-1-4

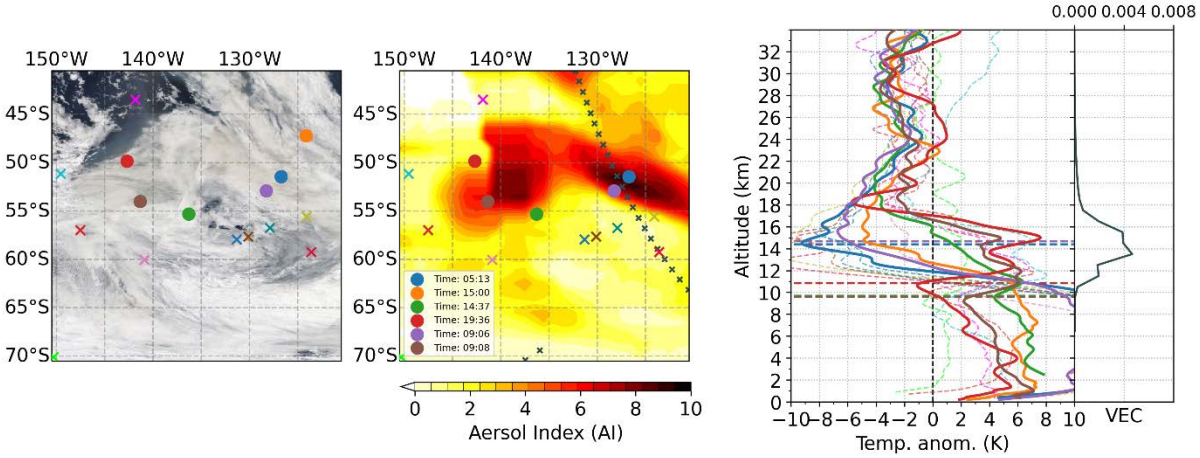

2020-1-5

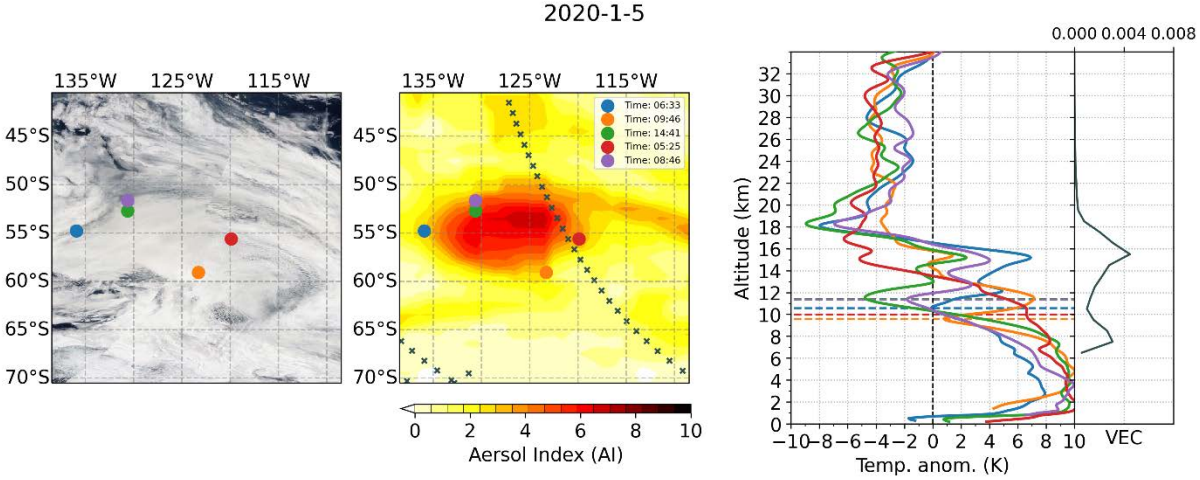

2020-1-6

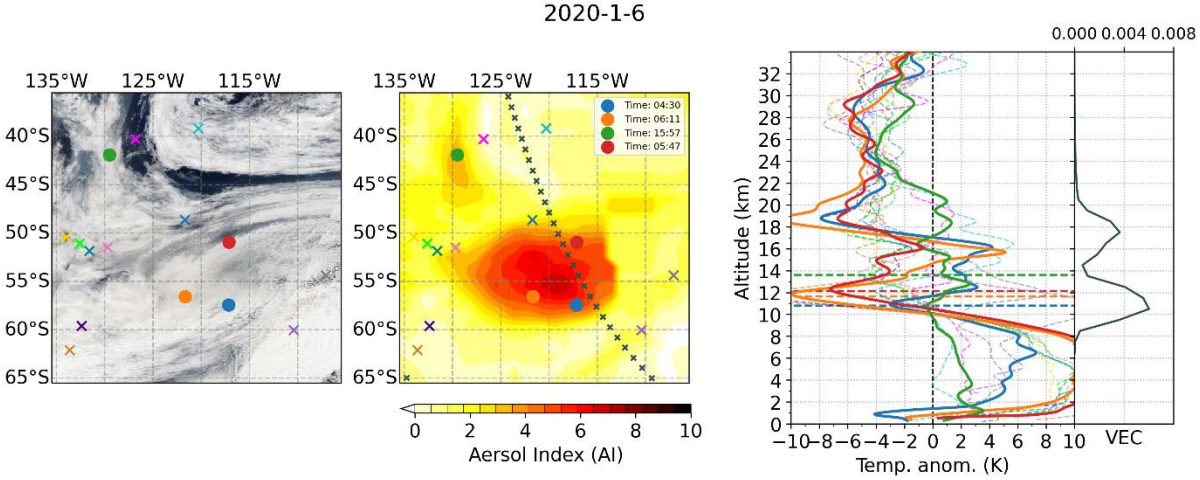

2020-1-7

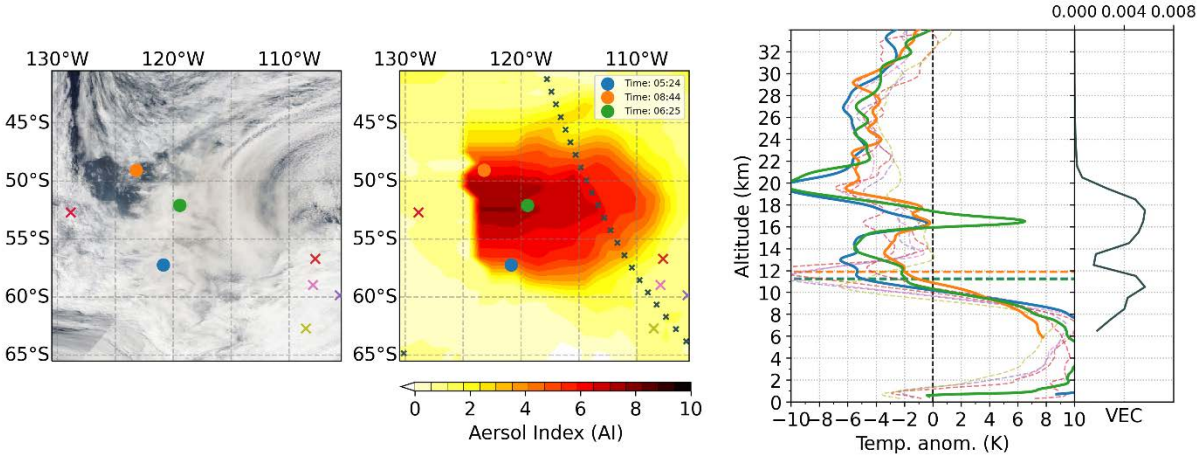

2020-1-8

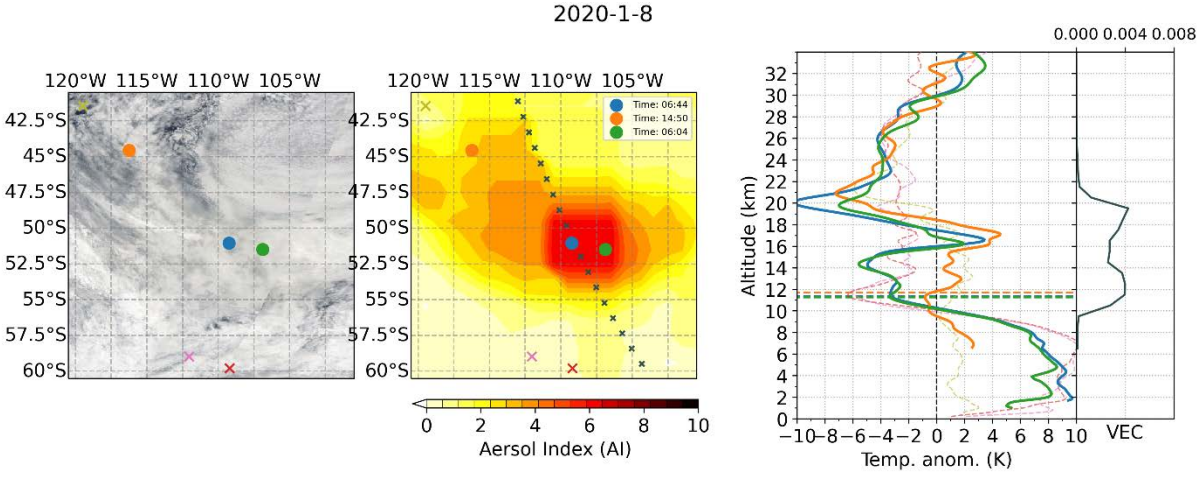

2020-1-9

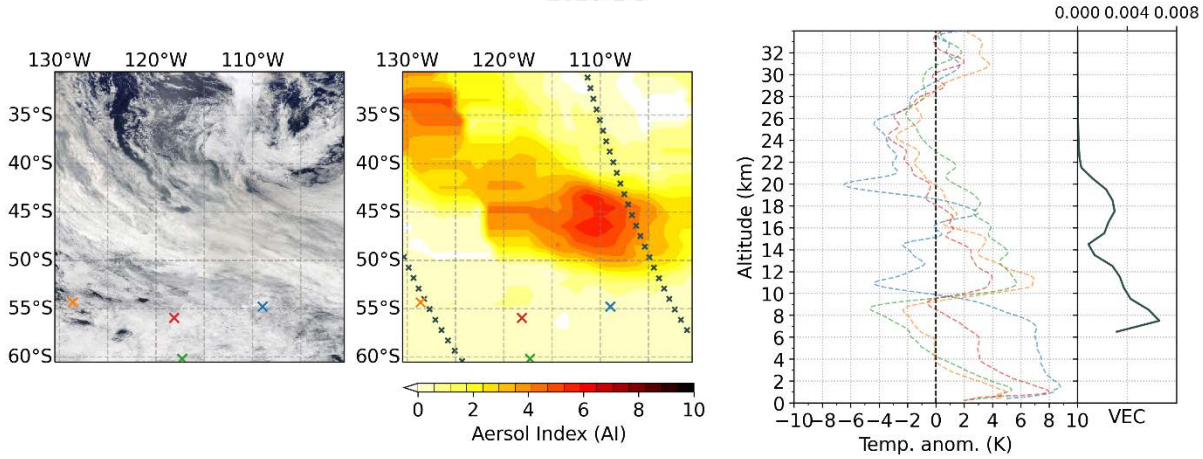

2020-1-10

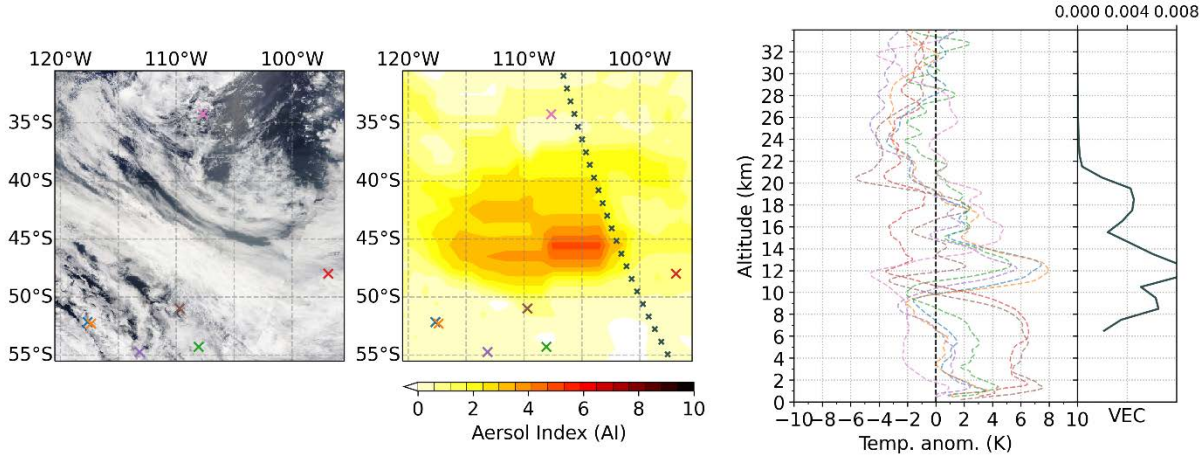

2020-1-11

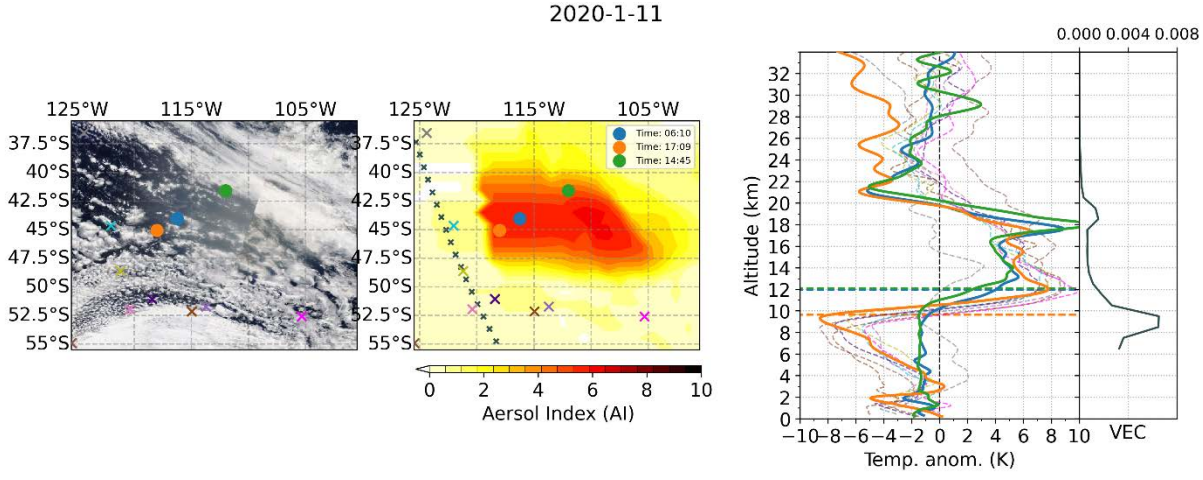

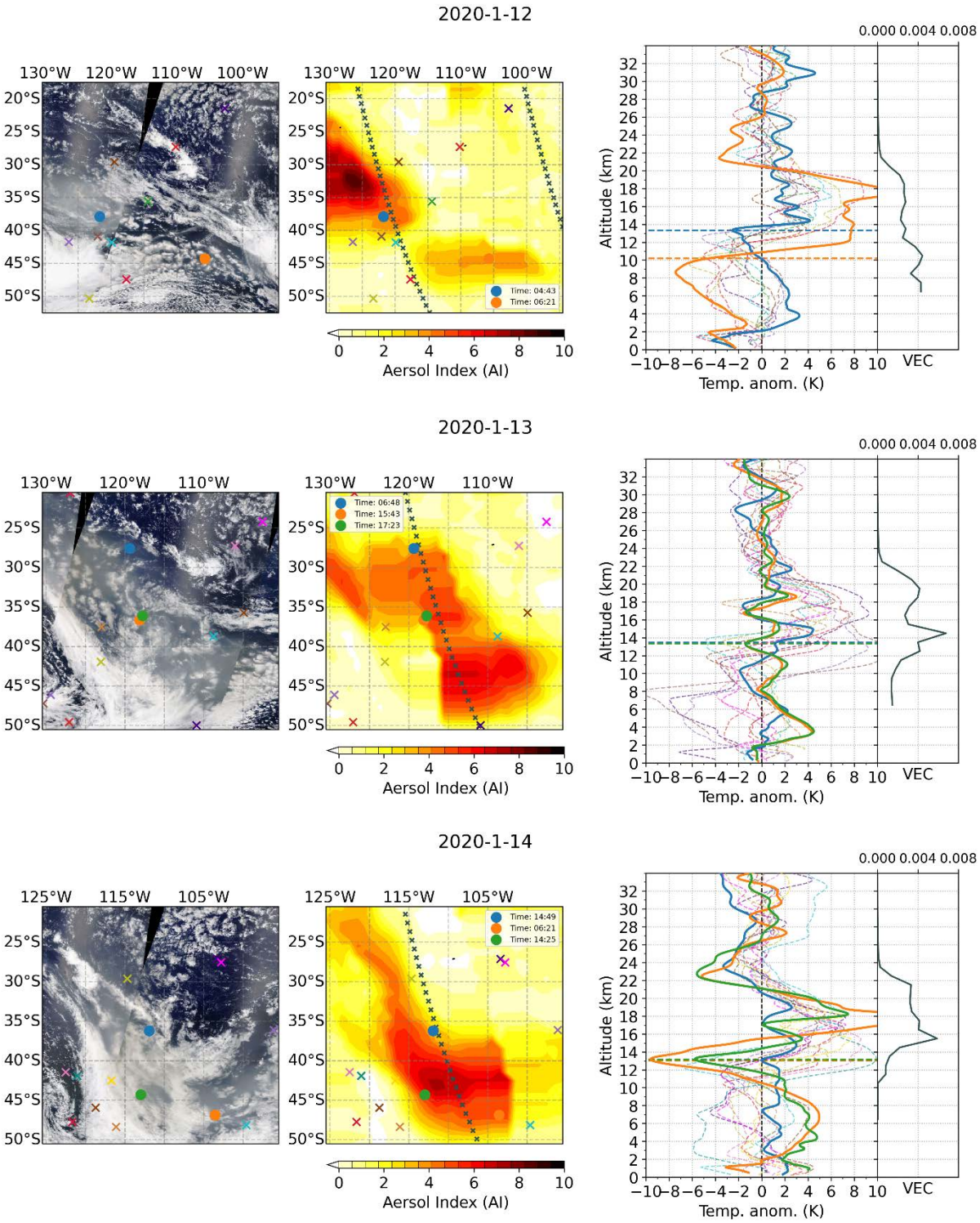
2020-1-12
130°W 120°W 110°W 100°W
20°S
25°S
30°S
35°S
40°S
45°S
50°S
Time: 04:43
Time: 06:21
0 2 4 6 8 10
Aersol Index (AI)
0.000 0.004 0.008
Altitude (km)
Temp. anom. (K)
VEC
2020-1-13
130°W 120°W 110°W
Time: 06:48
Time: 15:43
Time: 17:23
2020-1-14
125°W 115°W 105°W
Time: 14:49
Time: 06:21
Time: 14:25

2020-1-15

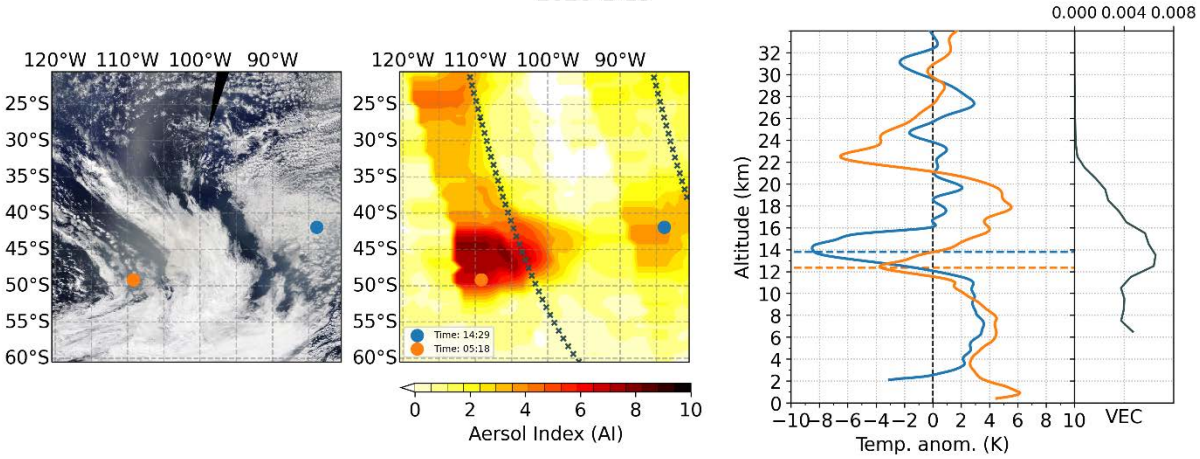

2020-1-16

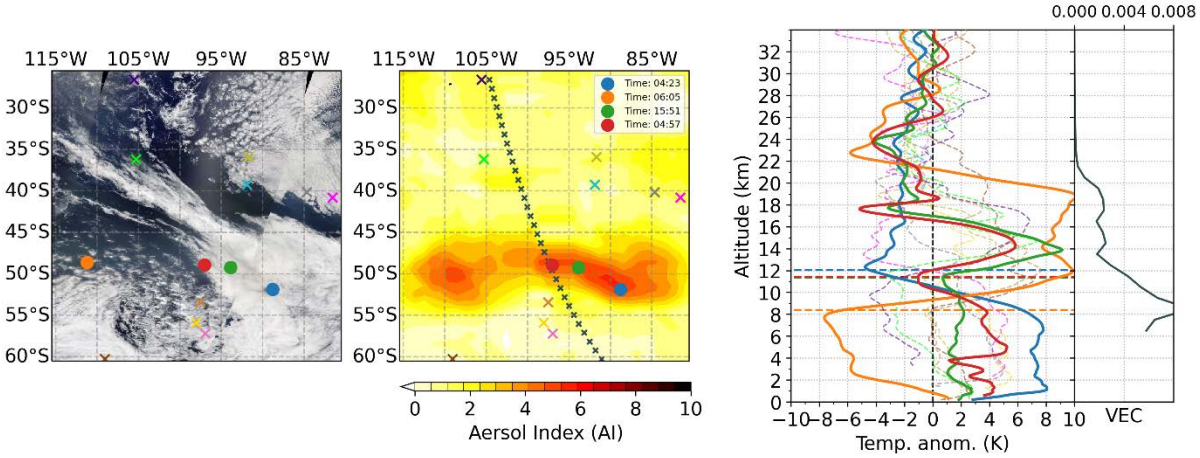

2020-1-17

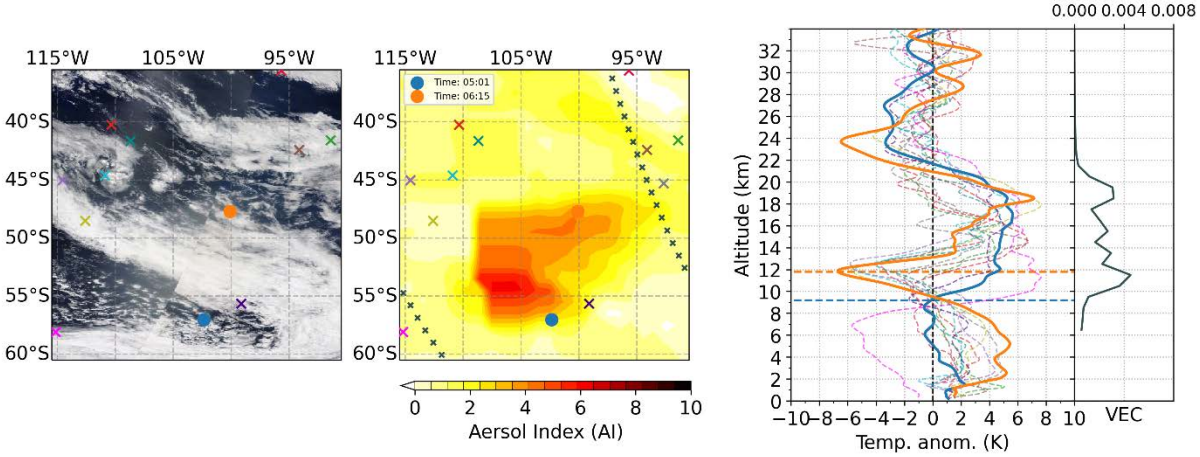

2020-1-18

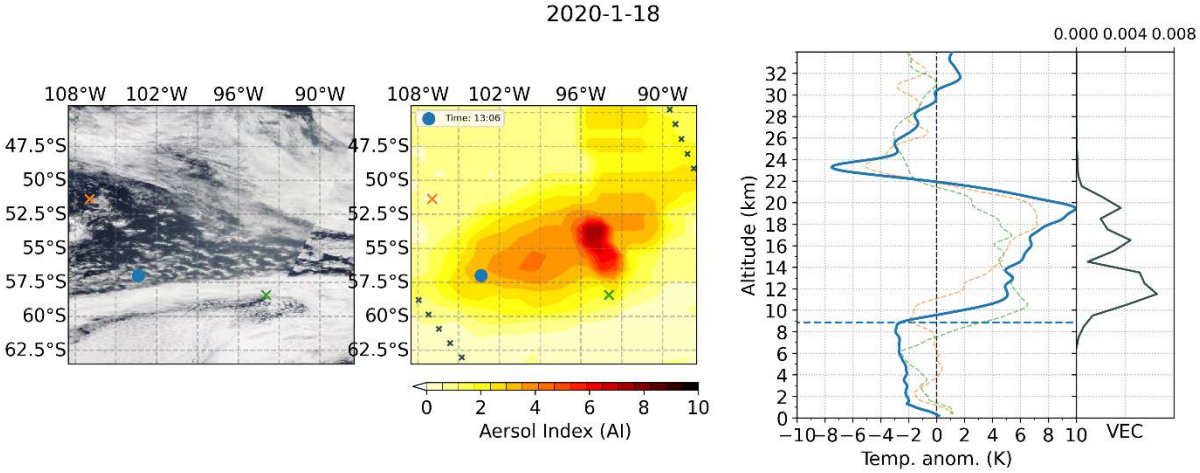

2020-1-19

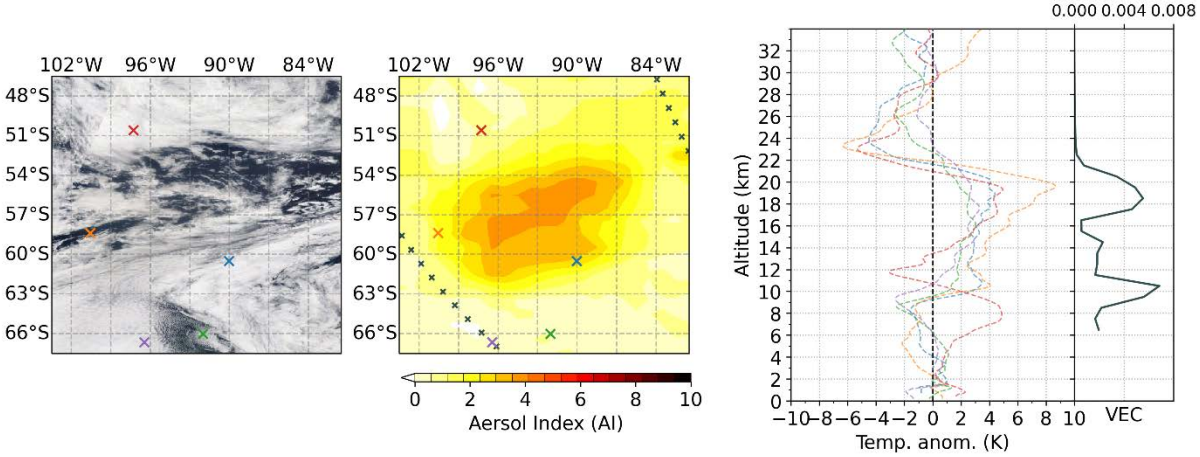

2020-1-20

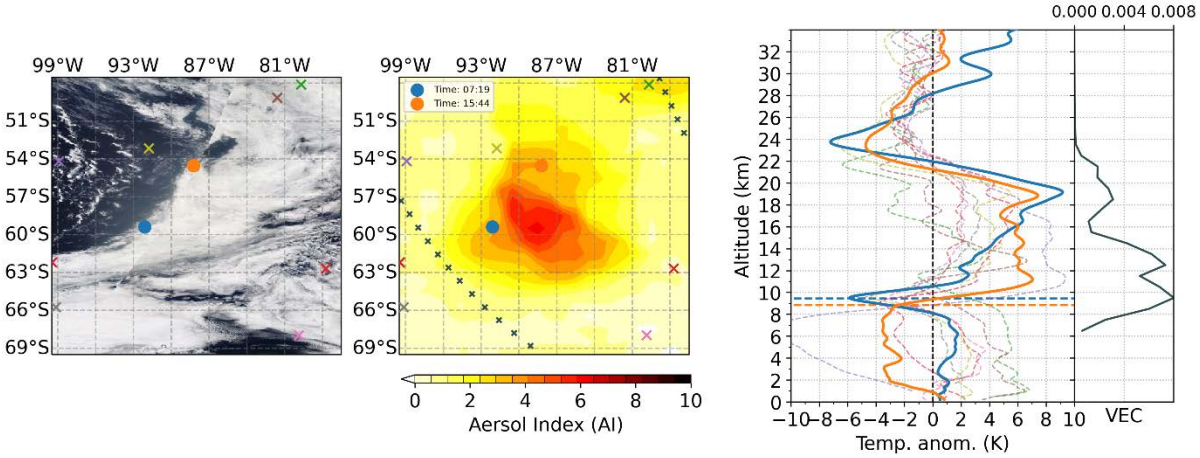

2020-1-21

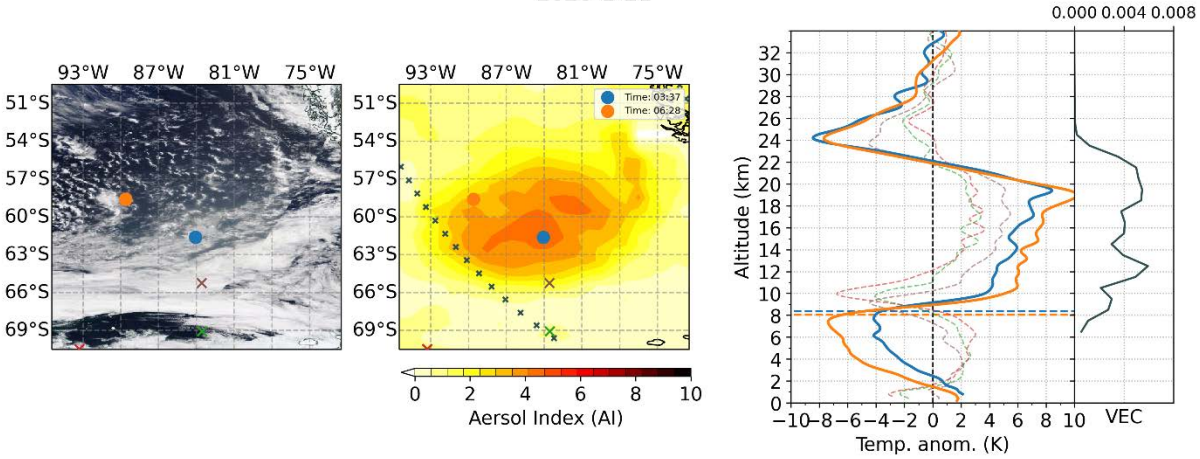

2020-1-22

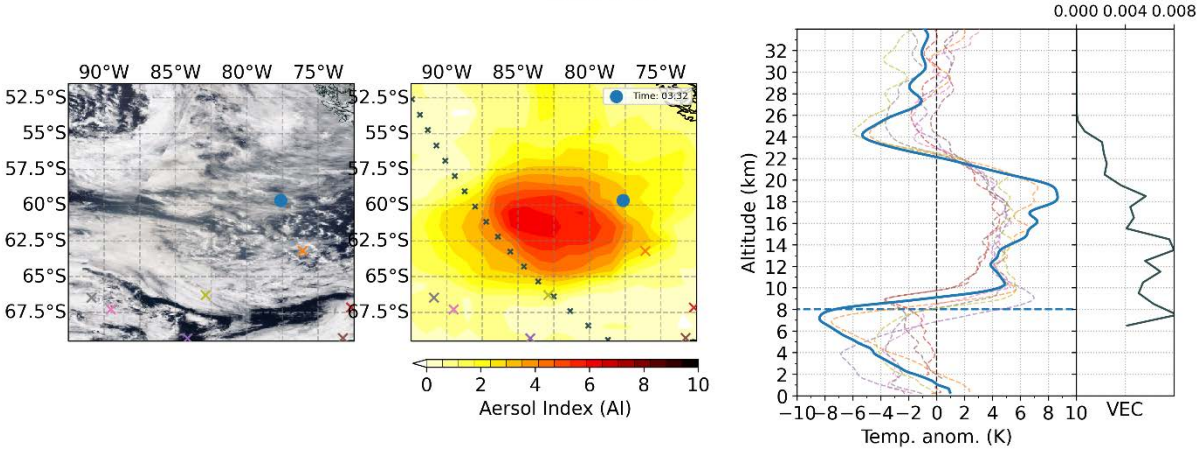

C. Short-term climate imprints from wildfires compared to volcanic climate signals

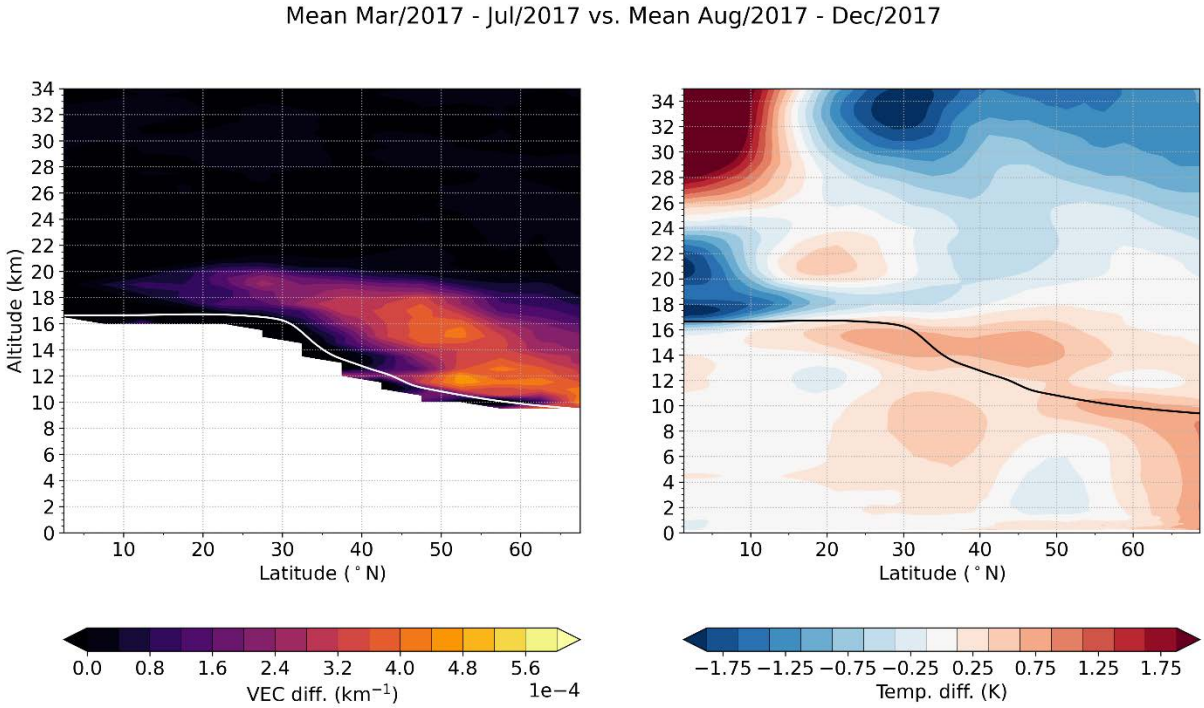

Figure 15: Short-term climate imprints of the 2017 Northern American wildfires calculated as the difference of the mean temperature five months before the event compared to five months after the event (including the month of the event).

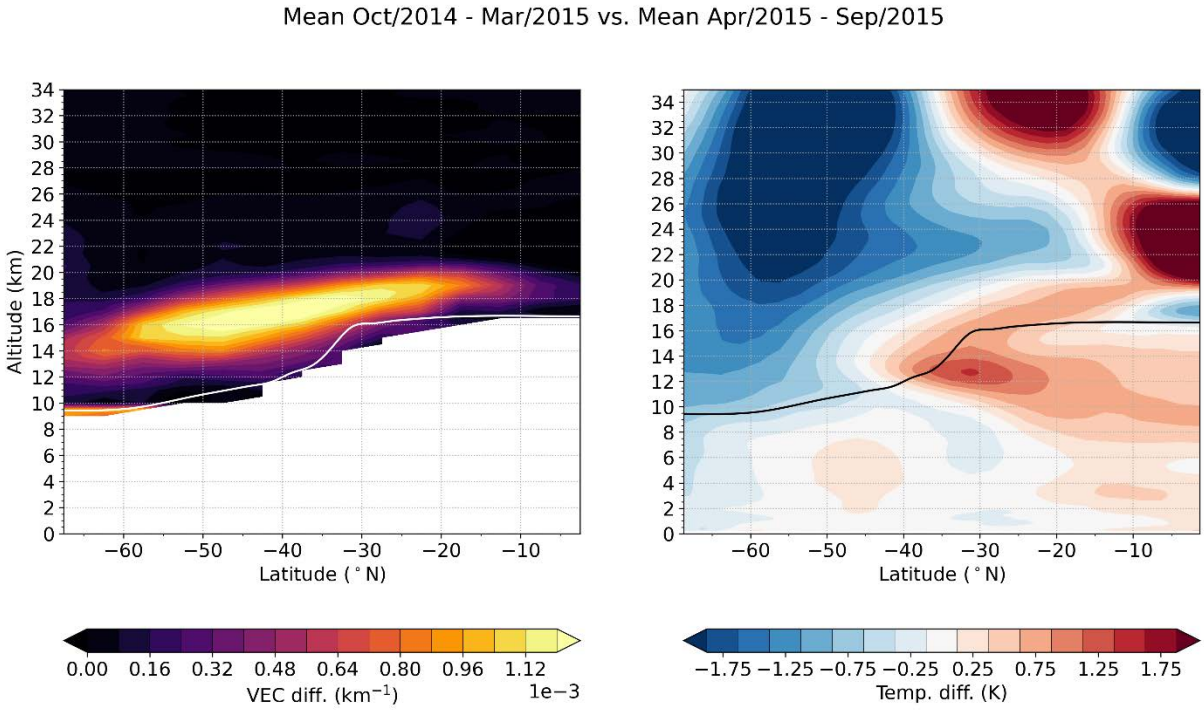

Figure 16: Short-term climate imprints of the 2015 Calbuco eruption calculated as the difference of the mean temperature six months before the event compared to six months after the event (including the month of the event).

.